Protein-Inspired Control over Synthetic Polymer Folding for Structured Functional Nanoparticles in Water

Chemistry Europe
European Chemical Societies Publishing

WILEY VCH

Excellence in Chemistry Research

Announcing our new flagship journal

- Gold Open Access
- Publishing charges waived
- Preprints welcome
- Edited by active scientists

Meet the Editors of *ChemistryEurope*

Luisa De Cola
Università degli Studi di Milano Statale, Italy

Ive Hermans
University of Wisconsin-Madison, USA

Ken Tanaka
Tokyo Institute of Technology, Japan

ChemPlusChem

Review
doi.org/10.1002/cplu.202300260

Chemistry Europe
European Chemical Societies Publishing

www.chempluschem.org

Protein-Inspired Control over Synthetic Polymer Folding for Structured Functional Nanoparticles in Water

Stefan Wijker[a] and Anja R. A. Palmans*[a]

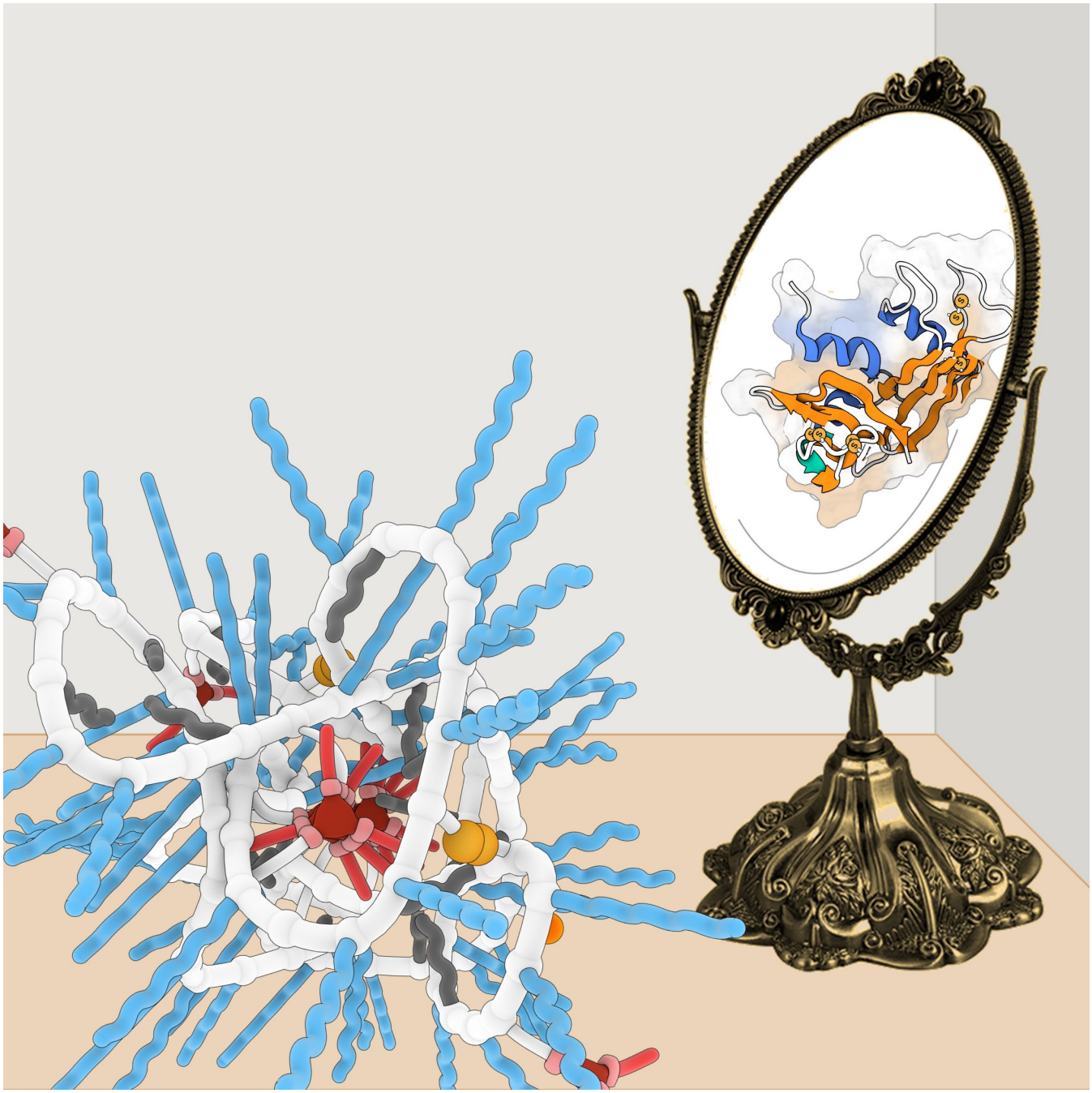

The folding of proteins into functional nanoparticles with defined 3D structures has inspired chemists to create simple synthetic systems mimicking protein properties. The folding of polymers into nanoparticles in water proceeds via different strategies, resulting in the global compaction of the polymer chain. Herein, we review the different methods available to control the conformation of synthetic polymers and collapse/fold them into structured, functional nanoparticles, such as hydrophobic collapse, supramolecular self-assembly, and covalent cross-linking. A comparison is made between the design principles of protein folding to synthetic polymer folding and the formation of structured nanocompartments in water, highlighting similarities and differences in design and function. We also focus on the importance of structure for functional stability and diverse applications in complex media and cellular environments.

1. Introduction

Only a century after Staudinger postulated the concept of macromolecules, polymer chemists gained access to a wide variety of polymerization techniques that enable control over nearly every aspect of a polymer's chemical nature such as length, molar mass dispersity, sequence, composition, and architecture.[1] These advances allow us to control the resulting material's morphological, thermal, and mechanical properties. As a consequence, materials are accessible that affect every aspect of our daily lives from clothing, insulation, and mobility to protection, packaging, and construction. Nevertheless, one challenge has remained, namely, to control the three-dimensional (3D) structure of a single synthetic polymer chain to impart a desired function. Like in proteins, the ability to control the global conformation of a single synthetic polymer chain permits the regulation and exploitation of polymer properties beyond that of the collective polymer level. Unlike in proteins, relating the polymer's chemical nature to the nature (size, shape, internal structure, stability) of a 3D structured particle is impeded by effects of dispersity and the difficulty to read off the primary structure of synthetically made polymers. Consequently, many avenues have been explored, in different fields of polymer science, to control the conformations of single polymer chains. However, depending on the field, the focus as well as the application areas differ. It is therefore timely to review the state-of-the-art in conformationally controlled synthetic polymers, how this compares to proteins, and how remaining challenges in controlling conformations of synthetic polymers can be addressed by learning from the advances made in the protein field.

We focus in this review on fully synthetic systems that collapse/fold into compartmentalized structures *in water*, to facilitate the comparison to proteins, but note that many elegant examples of conformational control have been attained in organic solvents, which have been reviewed elsewhere.[2–9] In addition, elegant work conducted in the fields of synthetic peptides[10] and protein/peptide-polymer hybrids[11,12] has been reviewed elsewhere and will not be part of this review. A particularly interesting class of synthetic polymers for which control over their 3D structure has been explored are the amphiphilic heterograft polymers (AHPs) – polymer chains with randomly distributed, different types of grafts.[13] AHPs were found to form small nanoparticles in water through hydrophobic collapse, combined with covalent and/or non-covalent interactions.[13] Variations in the polymer's length and microstructure has allowed the formation of nanoparticles of different shapes and sizes.[14,15] Typically, one polymeric nanoparticle consists of one polymer chain, which is referred to by different names such as single chain polymeric nanoparticles (SCPN[5,13] or SCNP[2,16,17]), unimolecular[18,19] or unimer[20,21] micelles, organic nanoparticles,[22,23] random heteropolymers,[24,25] or even amphiphilic folded copolymers.[26] The formation of polymeric nanoparticles bears resemblance to the folding of proteins in nature.[17,27,28] Other research areas focus on *sequence control* to mimic protein primary structure, and refer to the formed polymers as "sequence controlled/defined polymers" where a controlled or defined monomer sequence is present,[29,30] or foldamers, which are polymers with monomer sequences that form helical superstructures.[31,32]

Several reviews have focused on single chain polymeric nanoparticles in water,[13,33,34] but we here highlight the challenges involved in mimicking (the fundamental design of) proteins with the aim to access new applications of AHPs that arise from a controlled microstructure. To this end, we will first summarize current views on the folding of proteins into their native structures and how properties are derived from this 3D structure. Then, we will compare protein folding to the design, synthesis, and characterization of aqueous polymeric nanoparticles inspired by protein design. We will make the link between the properties of synthetic systems to proteins and highlight similarities and differences in design and function. Throughout the review we will use the nomenclature SCPN to refer to a collapsed/folded single synthetic polymer chain in water for consistency.

2. Proteins

2.1. Protein structure, folding and misfolding

Many processes that sustain life are controlled by the precise 3D structure of proteins, which provides crucial functions in

[a] *S. Wijker, A. R. A. Palmans*
Institute for Complex Molecular Systems
Laboratory of Macromolecular and Organic Chemistry
Eindhoven University of Technology
5600 MB, Eindhoven (The Netherlands)
E-mail: a.palmans@tue.nl

organisms such as transport of ions and small molecules, giving structure and stability to cells, transmitting signals between cells, catalyzing reactions, and guiding antibody binding to viruses and bacteria. Proteins are based on a linear sequence of L-amino acids connected via covalent peptide bonds. Each type of protein has a unique sequence of amino acids and a unique chain length. Because of the information embedded into this primary structure, local protein domains form via directional hydrogen-bonding interactions, such as α-helices and β-sheets, followed by further folding into a precisely defined 3D structure, stabilized via specific hydrophobic, hydrogen bonding, ionic interactions, and in many cases, disulfide bridges. The importance of this hierarchical folding process to the function of the protein, shown in Figure 1, was first recognized by Anfinsen. In his seminal work, the small protein ribonuclease A, with a native 3D structure stabilized by four disulfide bridges, was investigated.[35–37] Upon slow oxidation, the fully reduced and unfolded ribonuclease was found to fold back into its native 3D structure, reforming its four native disulfide bridges and regaining its catalytic activity. Fast oxidation in the presence of urea, in contrast, resulted in inactive ribonuclease A, because the randomly formed disulfide bridges prevented the protein from folding into its native 3D structure. These inactive species were readily converted into the native state in conditions where the disulfide bridges could reshuffle themselves. Taken together, these experiments showed that the primary sequence of proteins contains all necessary information to fold into the native state under appropriate conditions. It also showed that this state must be the thermodynamically most stable conformation, since wrongly folded states will readily convert to the native state when possible.[38]

What remained a mystery, however, were the mechanisms guiding the folding process into the native, active structure of the protein, which became subject of much debate in the ensuing years. Multiple effects were found to play a role in determining protein folding:[39] hydrogen bonding, hydrophobic interactions, electrostatic interactions, preferred backbone angles, van der Waals interactions, which all guide the folding process, complemented by a loss of chain entropy, which opposes the folding process.[40,41] Hydrogen bonding is the main driving force behind the formation of the secondary structures of α-helices and β-sheets.[42,43] In water, hydrophobic amino acids are preferentially buried inside the protein's core, shielded from the surrounding solvent water molecules, whereas the polar amino acids are preferentially located at the protein-water interface.[42,44,45] Positively or negatively charged amino acid residues result in attractive or repulsive electrostatic interactions. The polypeptide backbone of the protein prefers specific backbone bond angles. Upon folding into a compact globule, amino acids come so close together that van der Waals interactions start to play a significant role. Additionally, folding into a defined structure comes at the expense of chain entropy, as the possible configurations of the chain are severely restricted. However, the interplay between all these forces was difficult to assess based only on the primary sequence and a folding pathway did not easily emerge from it.

In 1968, Levinthal asked the question how proteins are able to fold so fast, despite the vast amount of possible conformations available to the unfolded protein.[46] It was postulated that proteins must follow a certain folding pathway towards their native state, as a simply random search could never find the native state on a feasible timescale. This became known as Levinthal's paradox and sparked research into elucidating the folding mechanisms of proteins,[39,47] which resulted in four general models to describe protein folding: the framework model, the hydrophobic collapse model, the nucleation and nucleation-condensation model,[48] and the energy landscape theory, shown in Figure 2.[49–52] In the energy landscape theory, proteins do not fold via a single pathway, but each chain takes random steps along a funnel-shaped energy landscape. Herein, the steps are taken downwards in energy, corresponding to the formation of favorable interactions, guiding the protein towards its native, lowest-energy state.[53] Hence, folding occurs via an ensemble of intermediate structures. The other models explain observed trends in the folding pathway by simplifying the types of interactions that play a role during the folding event as they arise through random sampling of the conformational space at the onset of folding. In the framework model, folding proceeds via the formation of secondary structural elements (α-helices and β-sheets) first, whereas the hydrophobic collapse model starts with the clustering of hydrophobic residues, and the nucleation and nucleation-condensation model considers an initial formation of a nucleation site around which the rest of the protein folds. These models have in common that the formation of favorable local interactions along the chain restricts the conformational space of the partially folded

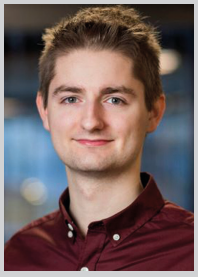

Stefan Wijker is a PhD student in the Supramolecular Chemistry and Catalysis group at the Eindhoven University of Technology. He does research into the folding of synthetic polymers into single-chain polymeric nanoparticles in water via combined covalent and non-covalent cross-linking, primarily interested in the effects of folding on particle size, shape, and stability.

Anja Palmans studied chemical engineering and received her PhD at the Eindhoven University of Technology on the supramolecular self-assembly of bipyridines. After her postdoctoral research at ETH Zürich (Switzerland) and research work at DSM Research (Netherlands), she returned to the Eindhoven University of Technology. Since 2019, she heads her own research group on supramolecular chemistry and catalysis, with a particular fascination towards aqueous and bio-orthogonal application of single-chain polymeric nanoparticles.

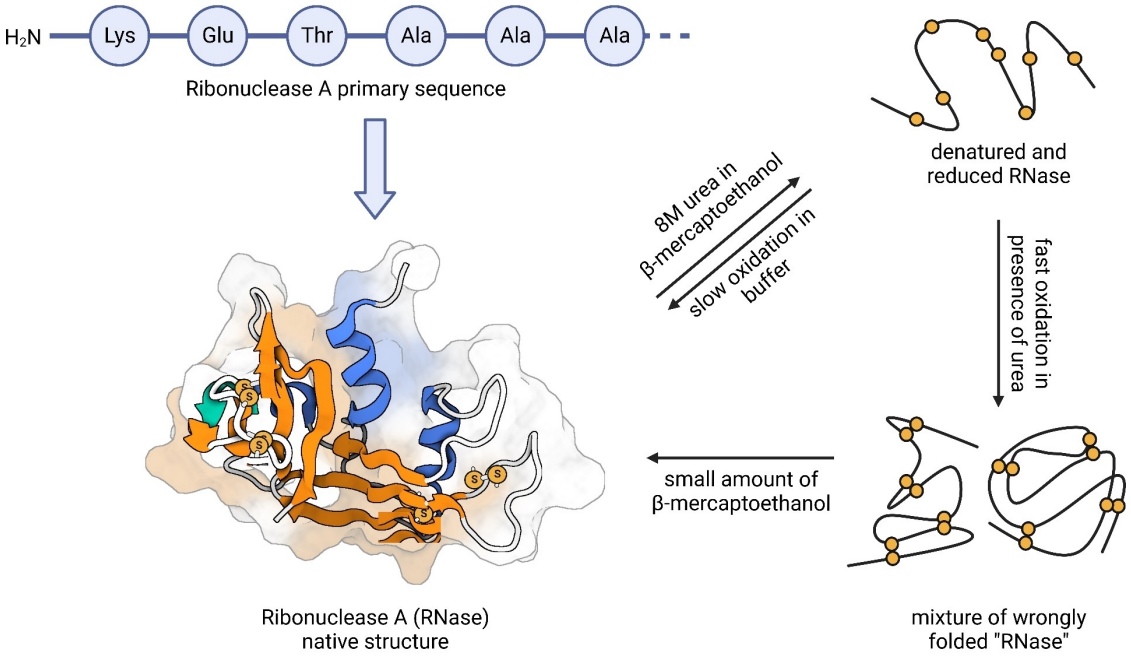

Figure 1. The amino acid sequence of the small protein ribonuclease A (RNase) contains all required information to fold into its native structure, which contains four-fold disulfide bridges (left). RNase shows a hierarchical folding process as first recognized by Anfinsen (right). Image created with BioRender.com.

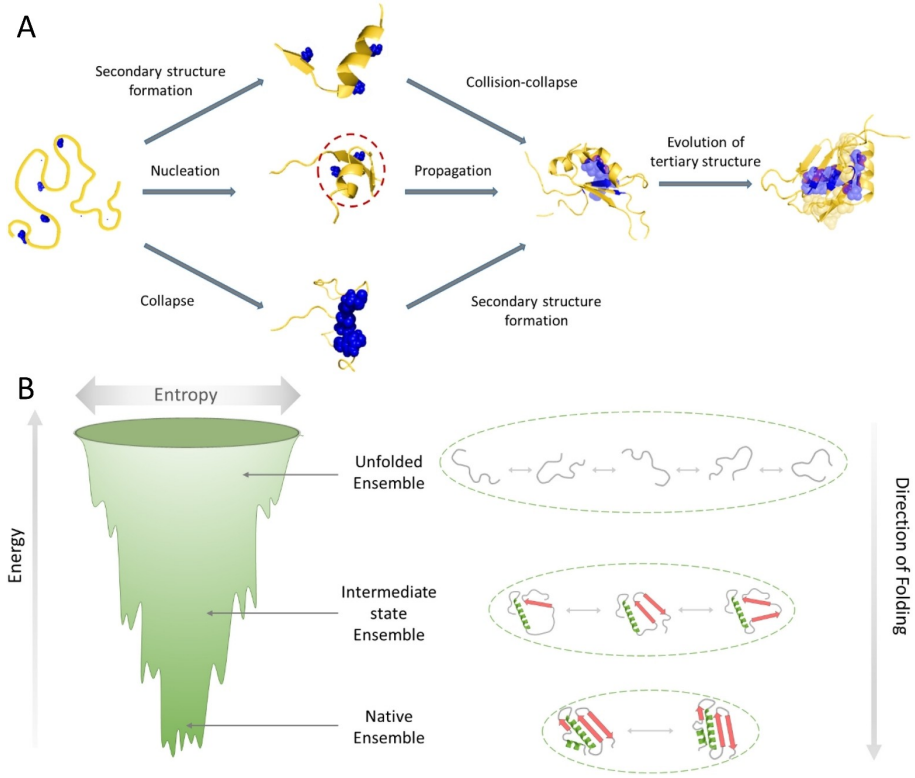

Figure 2. The four main protein folding models. A) In the framework model, folding proceeds *via* the formation of secondary structural elements (α-helices and β-sheets). In the hydrophobic collapse model, folding starts with the clustering of hydrophobic residues. In the nucleation and nucleation-condensation model, a nucleation site forms around which the rest of the protein folds. B) In the energy landscape theory, proteins take random steps along a funnel-shaped energy landscape towards its native, lowest-energy state. Reprinted from Ref. [49] with permission from Elsevier.

protein, guiding it down the energy landscape into increasingly compact, more energetically favorable conformations until finally the precise, delicate interplay between all the possible types of interactions define the precise native 3D structure. In the latest stages of protein folding, the structure is stabilized by the formation of short-range contacts (van der Waals, electrostatic interactions), exclusion of water from the hydrophobic core, and formation of disulfide bridges.[54,55] Hence, protein folding can be fast because a random search of conformational space quickly forms local advantageous interactions – be they hydrophobic, secondary structure, or nucleation-condensation guided in nature. This leads to partially folded structures such as a molten globule state,[56] which evolves along a downward funnel-shaped energy landscape into the globally folded, native state.

Simple sequence – 3D structure patterns in the folding of proteins were never found. Therefore, efforts focused towards developing computer algorithms, capable of predicting the native 3D structure of proteins from the primary sequence. Developments in this field were skyrocketed by the yearly CASP (Critical Assessment of protein Structure Prediction) event, in which different research groups displayed their newest structure predicting algorithms. The most successful algorithms all utilized the Protein Data Bank, which currently houses over 200 000 experimentally determined structures of proteins. Known structures for specific protein sequences are fed into the algorithm to predict the unknown structure of new, not yet seen protein sequences. Implied in these algorithms is that a similar sequence will result in a similar structure. For years, progress in structure-prediction was slow, until 2021 when AlphaFold was presented at CASP14.[57] It was the first algorithm that could accurately predict the full 3D structure of protein structures in the majority of cases, not only for sequences with similarities to known structures, but also for unknown sequences for which no similar structure was known. To achieve this, AlphaFold incorporates multiple aspects of protein structure knowledge into its machine learning algorithm. This allows the prediction of the structure of difficult proteins, including some where the proteins only fold in the presence of haem groups, or those where it can implicitly predict the presence of specific ions in the native structure. AlphaFold is the first successful computational method showing that information captured in the primary sequence of proteins can be utilized to predict native structures approaching atomic precision. In parallel, the development of better force-fields that allow simulating the energy landscape of proteins enables direct modelling of protein folding, although additional developments are still needed to improve the accuracy of the force fields and with it, the predicted structures.[58] However, despite the progress in prediction capabilities for folded protein structures made by AlphaFold, the model cannot explain how the proteins fold into their native state, nor give the required insight into which interactions encoded in the primary sequence are responsible for the obtained structure.

The efficiency of the folding process makes that folding into the native state can occur on short timescales. For example, single domain proteins fold in microsecond to millisecond timescales.[50,53,59,60] In general, there is no clear relationship between the chain length and the folding rates, but proteins that fold into native states with many local contacts between residues fold faster than those with a larger separation between contacting residues.[59] Additionally, a protein sequence seems to not be optimized for fast folding.[61] This is especially apparent for larger proteins that fold into structures with multiple domains. Whereas many small, single domain proteins fold into their native state in milliseconds with a 100% *in vitro* success rate, folding of larger proteins is often slower and less efficient.[62] While the primary sequence of proteins contains all information required to define the native state, many proteins need assistance to properly reach it. In fact, larger proteins often end up in kinetically trapped folding intermediates towards the native state as the energy landscape is often rugged, or form aggregates through interactions between exposed hydrophobic patches with other cell constituents.[63] This is not surprising, as the environment of cells is extremely crowded with other macromolecules, up to 40 wt%, which can strongly alter the protein's stability and interactions.[64] Proteins also need the correct environment to achieve proper folding.[65] In *in vivo* conditions, folding of these larger, multidomain proteins is controlled through a chaperone network of molecules guiding the folding process towards the native state.[62] For other proteins, the chaperone network is needed to prevent aggregation or reverse misfolding via for example isomerization of the backbone, or reshuffling of disulfide bridges.[65] Additionally, as translation of the protein on the ribosome is often slower than the folding process, larger proteins often start to fold while they are still being synthesized, which for many proteins is crucial to ensure they can fold into the native state. Other proteins, however, require chaperones to delay folding until after translation as they would otherwise misfold on the ribosome, or to disable function until the protein reaches the desired site.[55] Even with all these mechanisms in place, proteins still end up aggregating or terminally misfolding, which requires degradation by other cell components as they fail to pass the cells' quality checks.[65] Misfolded proteins sometimes can escape these checks, which can lead to protein aggregation, for example in the form of amyloid fibrils, resulting in disease. Some examples of diseases caused by protein aggregation include Alzheimer's, Parkinson's, type II diabetes, and prion diseases.[65–70] Amyloid fibrillation causing *e.g.* Alzheimer's or Parkinson's are generally seen as irreversible processes in *in vivo* conditions. Recently, the thermodynamics of amyloid fibril formation has been increasingly studied *in vitro*, which has shown that fibril formation is reversible under appropriate conditions. Revealing the thermodynamic landscape of amyloid fibrillation can hopefully help to understand why amyloid fibrils form and how this process might be reverted *in vivo*.[71,72]

Remarkably though, roughly 30–40% of proteins in eukaryotes do not adopt a well-defined folded structure in their native state,[73,74] a result of their flat energy landscape which lacks a clear energy minimum.[75] On average, these intrinsically disordered proteins (IDPs) contain more polar and charged amino acids, and hence are more hydrated in their native state

conformations. These proteins have long been understudied and have only gained much interest in recent years as their importance for the functioning of organisms has come to light.[76] IDPs are involved in many cellular processes such as chaperoning, targeting, and molecular signaling. They are not completely unstructured, but contain small transient structured regions that allow them to efficiently find their binding partners.[75] Weak intramolecular interactions in these regions result in a preference for a certain population of conformations.[76] These regions are dynamic and heterogeneous, enabling IDPs to bind to multiple partners, in contrast to most well-structured proteins.

2.2. Methods for protein characterization

Many methods have been developed to unambiguously characterize proteins, with each technique revealing a specific type of information.[77,78] The first step is the identification of the amino acid sequence and corresponding mass. Techniques such as gel electrophoresis, reverse phase liquid chromatography, and multiple blotting techniques can be used to separate, purify, and visualize the protein from complex mixtures.[79–81] The purified protein can then be sequenced to derive the primary structure via mass spectroscopy. Options include Edman sequencing, where amino acids are cleaved and analyzed one-by-one, and matrix-assisted laser desorption/ionization time of flight mass spectroscopy (MALDI-TOF-MS), where protein fragments are analyzed by peptide mass fingerprinting.[81] More recently, native mass spectroscopy, which allows for the analysis of the intact protein by mass spectroscopy, can additionally give information on the secondary and tertiary structure of proteins.[82] For small proteins, size exclusion chromatography can be used to derive the molecular weight.[83] Elucidating the structure of proteins is routinely done by crystallizing the proteins and measuring X-ray crystallography to determine the spatial position of all amino acids.[84,85] Techniques have been developed to characterize the structure of proteins that are difficult to crystallize such as membrane proteins and IDPs. These include nuclear magnetic resonance (NMR) to measure equilibrium protein structure and its dynamics,[84,86] in addition to following protein folding or interconversion between multiple conformational states.[87] Small-angle X-ray scattering (SAXS) in solution provides an average size (maximum size and radius of gyration) of IDPs,[88] but has also been used to follow the folding of proteins over time.[89] Using the average structure provided by NMR and SAXS as inputs, molecular dynamics simulations can be used to derive the individual conformations or folded states of such flexible proteins.[90,91] Aside from NMR, single molecule electron microscopy has also been used to analyze the structure of membrane proteins without the need to crystallize them.[92,93] Structured protein domains such as α-helices and β-sheets, their dynamics as well as changes to the structure in proteins as a result of *e.g.* binding events can be followed by circular dichroism (CD) spectroscopy.[94–96] Differentiating between stable and less stable protein domains is possible using hydrogen-deuterium exchange mass spectroscopy (HDX-MS), which monitors the change in mass of hydrogen atoms in accessible protein domains being exchanged with deuterium atoms.[97] Additionally, ultraviolet (UV) spectroscopy can reveal the environment of specific amino acids in the protein which absorb in the UV, such as the aromatic and sulfur containing amino acids.[98] Finally, the unfolded states of proteins and their folding mechanisms can be measured using fluorescence techniques such as Förster resonance energy transfer (FRET) which reveals the average distance between two labelled positions on the peptide sequence,[99] or differential scanning calorimetry (DSC), which reveals the thermodynamic stability of the protein.[100] Fluorescence spectroscopy using specific fluorescent labels is also routinely used to visualize or localize specific proteins or protein complexes in cells.[101] All in all, a well-developed toolset is available to identify protein sequence, molecular weight, secondary structure units, 3D structure and even dynamic behavior. Importantly, tools are available to determine the primary structure of an unknown protein, and hereby correlate this to the observed function.

2.3. Structure – function relationships in proteins

The properties of proteins are a consequence of the 3D structure of their native state, but at the same time this native state is not static for most proteins. For most classes of proteins, the surface properties and the structure of the active site, or binding pocket, determine which substrates they interact with. In some cases, multiple proteins come together to form a functional, structurally well-defined multimeric complex.[102] An important class of proteins showcasing function derived from 3D structure are enzymes, which catalyze the reactions that occur in cells. Enzymes derive their catalytic properties from the precise 3D structure of a defined catalytic pocket, whose shape and chemical environment are a perfect match to specific substrates and reactions. Binding of the substrate usually results in a change in conformation of the binding pocket, which is essential for proper functioning of the enzyme.[103] In the past, this was explained by the "lock and key" model and more recently by the "induced fit" model.[104] An alternative view is given in terms of the energy landscape, where substrate binding changes the energy landscape of the protein and thus a new structure is adopted.[104] Consequently, enzymes are highly optimized to catalyze one specific reaction for a specific (set of) substrates with high activity and stereospecificity in aqueous environment and at low temperatures. Slight changes to the catalytic pocket will greatly influence the ability of the enzyme to function properly. This can already occur through mutagenesis of a single amino acid in the primary sequence.[105]

One of the great advances in protein science is the ability to engineer enzymes with new or enhanced properties,[106–113] by changing their primary structure or introducing new metal ions capable of catalyzing specific reactions into protein scaffolds.[109,110,114] However, predicting function from a primary structure, or designing a structure with a specific function remains challenging.[115] New protein sequences can be gen-

erated by *e.g.* directed evolution[116–118] or site directed mutagenesis techniques[119,120] and selected on functionality,[121] leading to acceptance of new substrates,[122,123] new-to-nature reactions,[123–126] or enhanced properties such as thermal stability or resistance against solvent denaturation.[127,128]

3. Folding synthetic polymers into functional nanostructures

3.1. What do we really need to mimic proteins?

The first requirement of a synthetic system to mimic proteins in their natural environment is water-compatibility. For this, the polymer needs to contain hydrophilic residues. These can be neutral, such as poly(ethylene glycol)[129] or monosaccharide units,[130] but also cationic,[131] anionic,[132] or zwitterionic.[133] Next, the system needs to provide a compartmentalized structure, preferably with a hydrophobic interior that is protected from the bulk water. This interior can be used to encapsulate cargo or provide a hydrophobic environment for catalysts that are not compatible with bulk water, which is important for applications.

A prominent difference between proteins and synthetic polymers is that nature has perfect control over the polymer length ($Đ = 1$ exactly) and monomer sequence, whereas synthetic polymers are less well defined, resulting in molar mass dispersity in the polymer length ($Đ > 1$), and a distribution in monomer sequence for copolymers. For a specific type of protein, each copy will always form the same 3D structure and display identical properties. This is not the case for synthetic polymers, where the length and monomer sequence dispersity will result in a mixture of polymer chains, each with their own composition and properties. The question is whether synthetic systems require perfect control or if less control is sufficient to drive synthetic polymers to form stable, compartmentalized nanoparticles that are able to express a function.

One powerful driving force to collapse polymers into compartmentalized structures is hydrophobic collapse of hydrophobic residues attached to the polymer chain when brought into water. A particularly nice example that showed that hydrophobic collapse induces compact conformations was shown by Zuckermann and Khokhlov using sequence defined polypeptoids that were prepared using solid phase synthesis. Interestingly, protein-like behavior was observed in the collapse of polypeptoid polymers in water which comprised only two types of monomers, hydrophobic (H) and polar (P).[134] The HP model allowed polymer sequences to be computationally designed to fold into defined structures.[135] A sequence based on hydrophobic N-methylglycine and polar N-(2-carboxyethyl)glycine was indeed found to collapse in a much more compact conformation as predicted by the HP model compared to a repeating sequence with an even distribution of the monomers.[136] In fact, the designed "protein-like" sequence adopted a compact globule conformation in aqueous solution. Using a two-state model, the protein-like sequence showed a larger driving force for globule formation, and increased cooperativity for the collapse transition.

While a high degree of prediction was achieved for simple synthetic polymers comprising hydrophobic and hydrophilic residues only, the question remained whether a discrete structure and defined sequence is in fact needed to achieve a compartmentalized structure. Early studies on the behavior of amphiphilic polymers in water by McMormick and coworkers using copolymers of acrylamide with dimethyldodecyl(2-acrylamidoethyl)ammonium bromide (DAMAB), shown in Figure 3A, revealed a high tendency for intramolecular hydrophobic association when $< 5\,\%$ DAMAB was used. With 5 and 10 mol% of DAMAB, the copolymers comprised a microblocky structure, which promoted intermolecular association in water.[137] This intermolecular association was enhanced by increasing the length of the hydrophobic block and/or the number of blocks in the polymer chain. Later, studies by Morishima and coworkers revealed that in random copolymers of sodium 2-(acrylamido)-2-methylpropane-sulfonate (AMPS) and N-alkylmethacrylamides (C_xMAm) of different chain length X, shown in Figure 3B, intrapolymer hydrophobic interactions compete with electrostatic repulsion between AMPS units within a polymer chain.[18,138,139] If the hydrophobic content in the copolymer is low, the polymer chain will adopt an extended conformation characteristic of fully ionized polyelectrolytes in water. However, with an increase in the hydrophobic content (longer chain length or a decrease in the AMPS content), hydrophobic association occurred, resulting in a decrease in polymer size in aqueous solution. The polymer size further decreased by increasing the hydrophobic content even more, eventually collapsing into a highly compact structure that was referred to as a "unimer micelle", with the long alkyl chains kinetically frozen inside the collapsed structure. It was also found that the hydrophobic association occurs in a cooperative manner. Above a certain hydrophobic content threshold, the polymer-bound hydrophobic pendants associate more favorably, leading to a substantial increase in the formation of

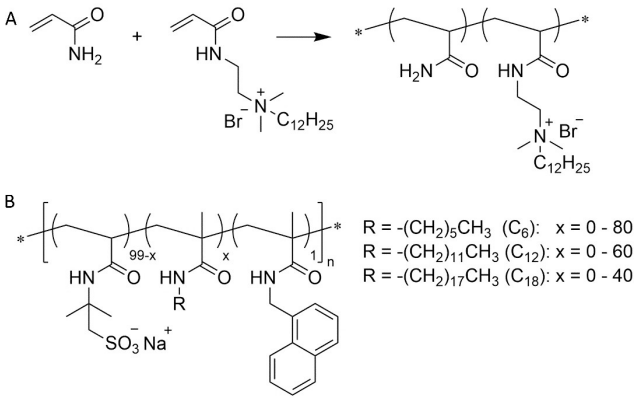

Figure 3. A) Chemical structures of the acrylamide and dimethyldodecyl(2-acrylamidoethyl)ammonium bromide copolymers used by McMormick and coworkers in Ref. [118]. B) Chemical structures of random copolymers of sodium 2-(acrylamido)-2-methylpropane-sulfonate (AMPS) and methacrylamides with different alkyl chain length or naphthalene moieties used by Morishima and coworkers in Ref. [18, 138, and 139].

hydrophobic domains in a relatively narrow hydrophobic content range. This is reminiscent of the behavior observed by Khokhlov and Zuckermann in peptoids, but in a non-discrete system with a random distribution of the grafts along the polymer chain.

Recent modelling studies corroborated that hydrophobic collapse induces protein-like behavior in random copolymers. Alexander-Katz and coworkers studied the collapse of random heteropolymers comprising hydrophobic, hydrophilic neutral, and hydrophilic charged monomers.[140] The copolymers collapsed into a molten globule morphology, with heterogeneous patchy surfaces, similar to proteins. In addition, the globules showed vitrified backbones and conformational patterns reminiscent of IDPs. In a follow up study, modelling of the heteropolymer's unfolding process showed that it involved highly complex side-chain interactions.[24] Instead of a defined collapse and unfolding transition, the unfolding gave rise to a complex, dynamic structure-property landscape.

3.2. Compartmentalized structures by hydrophobic collapse

The above results clearly show that there is no need for discrete length nor sequence defined structures in synthetic polymers to collapse into compartmentalized nanostructures with a hydrophobic interior. However, a proper balance between the hydrophobic and hydrophilic grafts is needed to tune intra- versus intermolecular aggregation and to ensure compact conformations. Terashima and Sawamoto performed detailed studies on neutral amphiphilic copolymers using PEG-substituted methacrylates and hydrophobic alkyl methacrylates as monomers.[141] A random incorporation of the monomers was ensured by a ruthenium-catalyzed living radical polymerization, where the feed ratio (composition) of the two monomers, the degree of polymerization (DP = 100 or 200), and length of the hydrophobic alkyl groups were systematically varied (Figure 4). The copolymers formed compact unimolecular micelles in water and comprised hydrophobic compartments. The random incorporation of long and/or bulky alkyl groups in the hydrophobic monomers was especially effective. The formed nanoparticles were dynamic, reversible, and stimuli-responsive in water; they unfolded via the addition of methanol and moreover became mobile upon increasing temperature.

Further investigations focusing on random copolymers of PEG-substituted methacrylates (PEGMA) and dodecylmethacrylates (DMA) revealed remarkable features of these amphiphilic copolymers.[142] Above a threshold degree of polymerization (DP), self-assembly switched from intermolecular to intramolecular, where the threshold DP increased with increasing amount of DMA. The copolymers below the threshold DP intermolecularly self-assembled into uniform nanoparticles with constant size and molecular weight, controlled only by DMA composition. In fact, the aggregation number (N_{agg}) of the copolymers (*e.g.* 2, 3, …, 12) was predictably controlled by DP and/or DMA composition, see Figure 5. The nanoparticles were thermodynamically stable in a wide range of concentrations (0.02–100 mg/mL) for over 4 months. Interestingly, for mixtures of aqueous solutions of nanoparticle with differing DMA content, *e.g.* 30 mol% DMA (DP = 103, N_{agg} = 1) and 50 mol% DMA (DP = 107, N_{agg} = 4.6), bimodal SEC curves were observed, where the respective peaks corresponded to the original nanoparticles. This highlighted that the two differently sized nanoparticles did not fuse together in water, but instead existed as self-sorted entities. Similar behavior was observed when mixing solutions of multichain aggregates of different composition, *e.g.* 50 mol% DMA (DP = 107, N_{agg} = 4.6) and 30 mol% DMA (DP = 56, N_{agg} = 2), where the SEC trace also showed two populations. Importantly, the observed self-sorting of copolymers to form nanoparticles of uniform size depended exclusively on the hydrophobicity (DMA composition) of the copolymer.

These systematic studies focused on the effect of side chain length and shape of the hydrophobic grafts. Also, the hydrophilic grafts were altered although studied with less rigor. Over the years charged AMPS,[143] different lengths of PEG methacrylate,[141] or the use of the longer Jeffamine@M1000 (3 propylene glycol units followed by 19 ethylene glycol units)

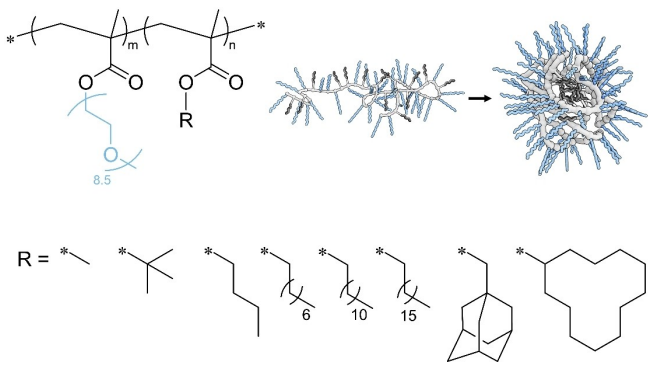

Figure 4. Chemical structures of copolymers of PEG-substituted methacrylates and hydrophobic alkyl methacrylates of different chain length and bulkiness. DP = 100 or 200. The ratio m/n = 160/40, except for R = dodecyl, where m/n varies from 200/0 to 100/100.

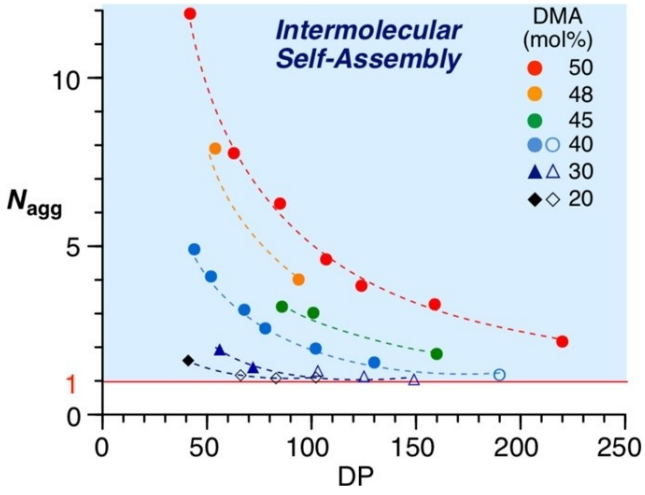

Figure 5. Self-assembly of random copolymers consisting of PEGMA and DMA into nanoparticles with controlled aggregation number N_{agg} as a function of DMA composition and chain length. Reprinted with permission from Ref. [142]. Copyright 2016 American Chemical Society.

have been applied.[144] Monosaccharides were also successfully conjugated to induce hydrophobic collapse as shown by the groups of Paulusse and Becer. This allowed preparing polymers for cellular uptake into HeLa cells[130] or for lectin recognition.[145]

The hydrophilic/hydrophobic balance of the polymer chain that controls the folding process can be easily tuned by increasing the length of the grafts, but longer grafts also cause other effects. For example, a poly(ethylene glycol) graft of 9 repeating units ($M_w = 450\ g\,mol^{-1}$) is already two times larger than tryptophan ($M_w = 204\ g\,mol^{-1}$), the largest proteomic amino acid. From a steric view, the size of the graft affects the maximum extent of collapse of the polymer chain, although no detailed studies into this relation have been conducted. It is therefore interesting to draw a parallel between SCPNs and bottle-brush polymers.[146,147] At high grafting densities using large grafts (which are smaller than the polymer backbone), bottle-brush polymers adopt elongated, worm-like structures in solution. Due to steric repulsion between the grafts, these polymers cannot fold into spherical particles. On the other hand, if the polymer backbone is in the same order of length as the grafts, the polymers are star-like, which will appear as spherical particles in solutions. With high steric penalties, an efficient reduction of size of the polymer chain upon folding will be prevented. This design parameter can have a large effect on the efficiency of the folding transition, but has been hitherto underappreciated in the molecular design of SCPNs.

3.3. Polymer backbone effects

Whereas nature has chosen amino acids as its monomeric building block, chemists can choose from a wide variety of building blocks to prepare polymers. Proteins are built up of main chain amide bonds, called peptide bonds. Therefore, proteins are capable of intra-backbone hydrogen bonding, which can play a key role in the folding of many proteins. In fact, some theories on protein folding consider peptide backbone hydrogen bonding as one of the most important driving factors for protein folding into its native structure.[148] The presence of intra-backbone hydrogen bonding was one of the factors behind Dill, Zuckermann, and coworkers to consider peptoids, which lack hydrogen-bond acceptors in its backbone, see Figure 6, as nonbiological polymer scaffolds to fold synthetic polymers into defined structures.[134,149] They successfully showed that synthetic sequence-defined polypeptoids could form tertiary structures in the absence of these specific backbone effects. In fact, subtle changes in the monomer sequence of sequence-defined peptoids affect the structure and extend of collapse in water via modulation of the peptoid amphiphilicity, flexibility, and hydrophobicity.[150]

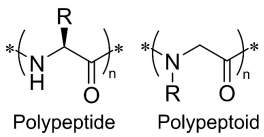

Figure 6. Chemical structure of polypeptides and polypeptoids, with and without backbone hydrogen bonding, respectively.

The current methodologies for synthetic heteropolymer synthesis allow for polymer synthesis using a wide variety of backbones. However, the choice for a particular backbone is almost never motivated in terms of folding properties. To the best of our knowledge, there has been only one study on the effect of the polymer backbone on SCPN folding, albeit in organic solvents and not in water.[151] This work showed that the nature of the polymer backbone, which was expected to lead to differences in flexibility, did not affect the SCPN formation as determined via DLS as well as by SEC. No significant changes in the ability to form SCPNs were found, suggesting that the polymer backbone has only a limited effect on SCPN folding in organic solvents. It is interesting to see if these findings hold in aqueous systems, where the collapse of the SCPN is often driven by the hydrophobic effect.

3.4. Monomer sequence effects

Whereas proteins adopt defined 3D structures as a result of their defined primary sequence, in synthetic copolymers the monomers are distributed randomly along the polymer backbone. This statistical distribution leads to the formation of SCPNs where individual SCPNs all uniquely differ from each other. The resulting nanoparticles form an ensemble with average properties defined by the distribution of the population. A non-random monomer distribution might affect folding and change the SCPN properties.

Tribet and coworkers prepared amphiphilic copolymers consisting of sodium methacrylate and octyl methacrylate.[152] Polymers with a random backbone distribution of the monomers folded intramolecularly into spherical nanoparticles consisting of one to two polymer chains. When the monomer distribution was blocky however, intermolecular aggregation dominated, and the polymers folded into multi-chain aggregates. From the increase in the shape factor $\varrho = R_G/R_H$, it is likely that these multi-chain aggregates formed elongated structures instead of spherical ones. In the work by Sawamoto and coworkers on the effects of hydrophobic graft length on SCPN self-assembly discussed earlier, the authors also prepared chains with a block copolymer architecture.[141] In agreement with the work of Tribet, the block copolymers did not form SCPNs, but formed large multi-chain aggregates instead, with an $R_H >$ 100 nm compared to the single-chain R_H of 13 nm in dichloromethane.

Terashima and coworkers prepared copolymers with PEG and dodecyl grafts with either a random, gradient, bidirectional gradient, or blocky distribution of the grafts along the backbone, see Figure 7.[129] The random copolymers with low degree of polymerization (DP = 30–60) self-assembled into size-controlled nanoparticles consisting of multiple polymer chains with small uniform sizes as determined by SEC and MALLS. Both methacrylate-based and acrylate-based random copolymers folded into small nanoparticles, although the internal flexibility of the PEG and dodecyl grafts was higher in the acrylate

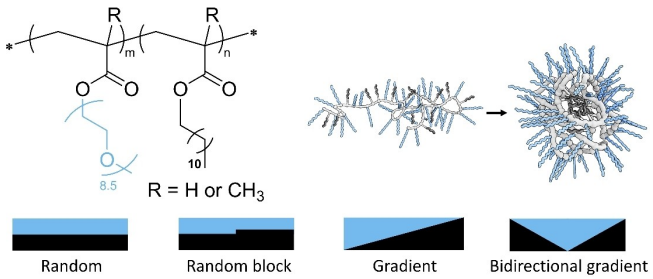

Figure 7. Chemical structures of PEG and dodecyl (meth)acrylate copolymers. The copolymerization resulted in random, gradient, bidirectional gradient, or random block copolymers. The polymers show hydrophobic collapse in water.

counterpart. Also here, chains with a strong gradient or blocky distribution of the grafts and relatively high number of hydrophobic grafts formed nanoparticles with poorer control over the resultant size, resulting in broader size distributions and overall larger R_H, consistent with previous work.[153]

3.5. Introducing internal structure into compartmentalized nanoparticles

In the above examples SCPN collapse was driven by hydrophobic collapse *via* hydrophobic side chains grafted to the desired polymer backbones. To induce *structure* into the hydrophobic compartments, and hereby create better defined inner compartments, one can take advantage of hydrogen-bonding groups that form secondary structure elements within the SCPNs. This can be achieved through the inclusion of chiral assembling moieties to provide a chiral inner environment.[150,154–156] Terashima *et al.* prepared a library of copolymers consisting of PEG methacrylate (PEGMA) and 1,3,5-tricarboxamide (BTA) methacrylate (BTAMA), see Figure 8A.[157] BTA is functionalized with chiral hydrophobic grafts, which self-assemble *via* three-fold hydrogen bonding between the amide units around the benzene core into a helix with preferred handedness (Figure 8B), thereby forming a structured hydrophobic compartment. In dilute aqueous solutions, the copolymers folded into SCPNs. By using temperature-dependent CD spectroscopy, the size of the CD effect was found to decrease with increasing temperature and at 90 °C disappeared, indicative of full disassembly of the BTAs (Figure 8C). The melting temperature increased with increasing local BTA concentration (percentage of BTA grafts on the polymer chain) and was independent of the total BTA concentration. Fitting of the melting curves revealed that the formation process of the structured hydrophobic compartments followed a two-state folding process, reminiscent of the thermal denaturation process in proteins and peptides. Positive changes in the heat capacity suggested that BTA units were exposed to water during the unfolding process, indicating successful formation of hydrophobic pockets and their subsequent disappearance upon unfolding at increased temperature.

In a follow-up study, the effect of chain length (DP = 110–450) on the folding behavior of 10 mol% BTAMA and PEGMA random copolymers into SCPNs was investigated.[14] Temperature-dependent CD spectroscopy showed that BTA self-assembly was independent of chain length, corroborating the sole dependence of folding on local BTA concentration observed in the previous study. Additionally, SAXS and SLS showed that SCPNs with increasing DP folded into increasingly elongated particles with an increasing aspect ratio but a constant cross-sectional radius (R_{cs} = 1.5 nm). This rationalizes the observed non-cooperative folding behavior, as the local BTA concentration after folding into elongated particles remains constant.

Later systematic investigations incorporated hydrophobic dodecyl groups to assess their impact on BTA intramolecular aggregation. The results showed that small changes in the incorporation ratio of hydrophobic grafts had a pronounced effect on the folding process.[144] With 10 mol% or less BTA, polymer chains folded intramolecularly into SCPNs, whereas above 10 mol% BTA, multi-chain aggregates were formed. Incorporating dodecyl grafts in addition to the BTA grafts favored intramolecular collapse into more compact, globular nanoparticles. Importantly, dodecyl incorporation aided BTA self-assembly, resulting in more structured compartments.

Knight and coworkers synthesized amphiphilic copolymers with pendant dipeptides or peptides based on phenylalanine (F) and alanine (A).[158] Also here, CD spectroscopy proved useful to assess the hydrogen-bonding and aromatic interactions in stabilizing the local structure. CD spectra revealed that the pendant FF units showed more pronounced β-sheet-like

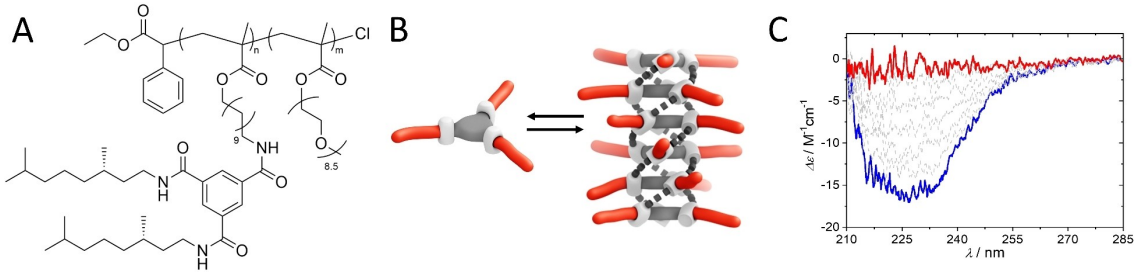

Figure 8. A) Chemical structure of random copolymers of BTAMA and PEGMA. B) Self-assembly of chiral BTA monomers into helical stacks with preferred handedness. C) Corresponding CD signature of BTA self-assembled into stacks at room temperature (blue) and absence of CD signal of disassembled BTA at elevated temperature (red).

interactions compared to pendant F units. Installing the phenylalanine further away from the polymer backbone by attaching AF dipeptide resulted in an increase in flexibility, leading to increased formation of more collapsed structures. The degree of β-sheet-like interactions, however, was retained. The results clearly showed that β-sheet-like local structures were formed when collapsing the amphiphilic polymers into single-chain assemblies in aqueous environments.

3.6. Kinetic effects in the formation of compartmentalized structures

Like in proteins, it is expected that the pathway in which the particles are prepared matters, and that kinetic effects can play a role in attaining the most stable conformations. Morishima and coworkers conducted an in-depth study on different preparation procedures for the intramolecular folding of their random copolymers consisting of AMPS and C_{12}Mam, a charged water-soluble monomer and linear hydrophobic monomer, respectively. The preparation protocol played an important role in controlling the particle size as measured via DLS in the resulting polymer solutions, see Figure 9.[159] In dried form, kinetically trapped multichain particles may exist through hydrophobic association and entanglements between polymer chains. Upon dissolution in 0.2 M sodium chloride, these multichain aggregates will persist, resulting in a solution with large average particle sizes (R_H = 25.5 nm). To remove this sample preparation history, simply dissolving the polymer in water and heating it up to 90 °C efficiently disassembled the kinetically trapped aggregates. Subsequently cooling down the solution resulted in solutions containing only single-chain polymeric nanoparticles. The smallest particle sizes, and thus the most compact nanoparticles, were obtained when the ionic strength of the solution was adjusted by addition of 0.2 M sodium chloride before cooling down (R_H = 6.1 nm). If the polymer was dissolved immediately in salt solution, disentanglement of the multi-chain aggregates was less efficient than in pure water (R_H = 7.5 nm). Hence, both the sample preparation procedure and sample history matter greatly in controlling the folding of polymer chains into compact SCPNs.

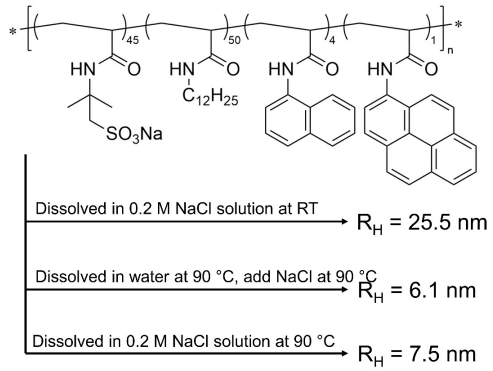

Figure 9. Chemical structure of the AMPS and C_{12}Mam random copolymers, containing a small amount of naphthalene and pyrene probes. Dissolving the dry polymer in salt solution at room temperature results in large particles, whereas dissolution at elevated temperature disassembles preexisting aggregates and results in the formation of small nanoparticles.

The importance of the sample preparation procedure was also shown for polyacrylamide polymers consisting of the hydrophilic polyether Jeffamine@M1000, and hydrophobic BTA grafts, which self-assemble via triple hydrogen bonding into helical stacks.[144] Consistent with the findings by Morishima and coworkers, the polymer's history played an important role in attaining single chain rather than multi-chain particles. To prepare aqueous SCPN solutions, the kinetically trapped self-assembled BTA grafts of the solid polymer needed to be removed, see Figure 10. Two essential steps were investigated, namely heating of the polymer solution to 80 °C and sonication of the polymer solution, both intended to disrupt the inter-polymer interactions and remove the polymers history. Only heating or sonication of the solutions was unsuccessful to prepare purely single-chain polymeric nanoparticles, as DLS showed the presence of large particles (R_H > 100 nm). The best sample preparation protocol consisted of first sonicating the polymer solutions for 30 minutes to disentangle the multi-chain aggregates, followed by heating the solution to 80 °C for 30 minutes, to disrupt the BTA hydrogen-bonding. Subsequently, the solutions were cooled down slowly, to allow time for the polymers to fold into SCPNs, resulting in an average particle size of R_H = 5 nm. Therefore, if SCPNs are prepared in solvents that are not a good solvent for all monomers and the polymer backbone, removal of kinetically trapped aggregates is

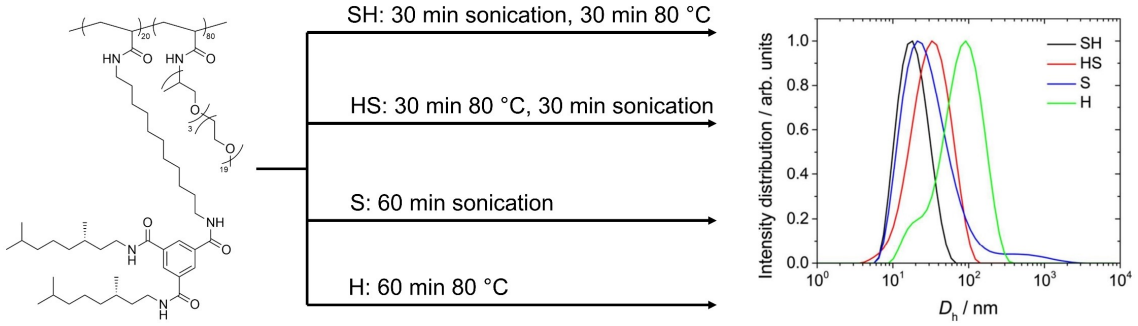

Figure 10. Chemical structure of polyacrylamide-based random copolymers with Jeffamine@M1000 and chiral BTA side-chains. Preparing aqueous solutions *via* sonication, heating, or a combination thereof results in the formation of nanoparticles with differing size distributions as probed via DLS.

crucial to allow the polymers to exclusively fold into single-chain nanoparticles.

All studies above show that the microstructure of the copolymer – DP, nature of hydrophobic units, composition of the monomers, distribution of the monomers, and sample preparation – determines the ability of a single polymer to collapse into a single polymer nanoparticle.

3.7. Enhancing the stability of SCPNs by covalent cross-linking

So far, we have focused on non-covalent strategies to collapse/fold polymers into SCPNs. These interactions include hydrogen bonding, either self-complementary[14,15,144,155,160] or cross-complementary,[161] π-stacking,[154] host-guest interactions,[162] or metal-ligand interactions.[131,163,164] The advantage of using non-covalent interactions to drive chain collapse is the high degree of dynamicity, which provides opportunities to use stimuli to control the folding process. However, Anfinsen was the first to show that the folding of the simple protein ribonuclease A occurred not only via noncovalent interactions, but also by covalent interactions using disulfide bridges, where the order of events was crucial in reaching the native state.[37] Many covalent chemistries have been developed to collapse polymer chains on their own in water.[165–173] By instead incorporating low amounts of cross-linkable units, they will not drive chain collapse on their own upon cross-linking, but will stabilize the already folded structure.[174,175] As such, combining covalent with non-covalent strategies can prevent unfolding of the particle and subsequent loss of the internal pocket and/or structure, resulting in *e.g.* the deactivation of embedded catalysts, or premature loss of cargo or other functionality.

We have recently shown this for SCPNs formed through a combination of noncovalent interactions (hydrophobic and structure-forming hydrogen-bonding interactions between BTA units) and covalent intramolecular cross-linking of 7-hydroxy-4-methylcoumarin using a light-induced [2+2] cycloaddition.[175] Inspired by the two different folding pathways investigated by Anfinsen, we applied the same principle to our synthetic polymeric system **P1**, see Figure 11. Analogous to ribonuclease A, when covalent coumarin dimerization precedes SCPN formation via hydrophobic and supramolecular interactions in water, larger particles with less structured hydrophobic compartments are formed. When the order of events is reversed and the polymer chains are first folded via the hydrophobic and supramolecular interactions in water, followed by the formation of the coumarin dimers, smaller particles with more structured hydrophobic compartments are obtained. In this approach, cross-link formation is used to stabilize, or "lock in" the folded

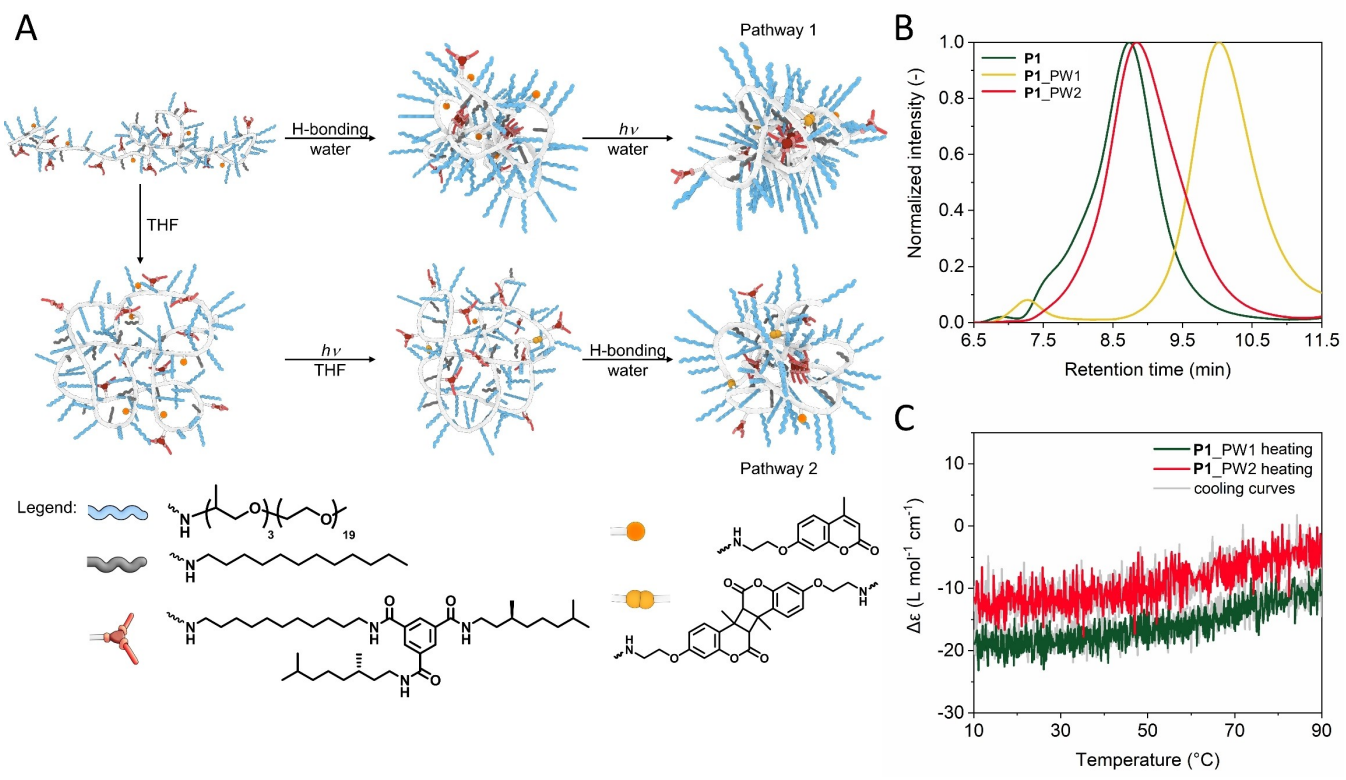

Figure 11. A) Schematic view of folding pathways of amphiphilic heterograft random copolymer **P1** consisting of Jeffamine@M100 (blue), dodecyl amine (grey), BTA-amine (red), and 7-hydroxy-4-methylcoumarin-amine (orange) sidechains. In pathway 1 (top path, PW1), folding into SCPNs *via* hydrophobic and supramolecular interactions in water is followed by coumarin dimerization (yellow) to lock the conformations. In pathway 2 (bottom path, PW2) covalent coumarin dimerization precedes SCPN folding in water. B) The SCPNs formed *via* pathway 1 form smaller, more compact particles than those prepared *via* pathway 2 as probed by SEC-PBS and C) form more structured hydrophobic compartments as probed by CD spectroscopy. Image adapted from Ref. [175] licensed under CC BY 4.0.

structure of the SCPNs. The smaller size of these SCPNs was corroborated using a combination of DLS and SEC, while the more structured compartments was apparent via the higher BTA self-assembly as probed by CD spectroscopy. Using Nile Red fluorescence spectroscopy in complex media and monitoring the loss of internal structure at elevated temperature in the presence of hydrogen-bond competitors, it became clear that the formation of covalent cross-links after SCPN folding enhanced the structural and thermal stability of the SCPNs. This study highlighted that control over the folding pathway is also crucial for the design of stable SCPNs, and not only for proteins.

Zhang *et al.* showed the possibility of fixing various conformations of thermo-responsive N-isopropylacrylamide-based polymers in water.[167] The thermo-responsive precursors adopted more open conformations at low temperatures and more collapsed states at high temperatures. Subsequent covalent cross-linking reactions at the different temperatures permitted the covalent locking of the obtained conformations by cross-linking 4-acryloyloxybenzophenone (ABP) units and tuning the obtained SCPNs from loosely packed particles to collapsed globules.

This approach of first folding the polymer into compact SCPNs by hydrophobic interactions, followed by cross-linking to "lock in" the folded structure has also enabled the preparation of multi-compartment SCPNs with two distinct domains. Sawamoto and coworkers prepared synthetic random copolymers consisting of two blocks, where in addition to the hydrophilic PEGMA and a small amount of olefinic cross-linker dispersed throughout the entire chain, the first block incorporated hydrophobic dodecyl grafts, while the second block incorporated benzyl grafts instead.[174] Hydrophobic collapse of the polymers in water resulted in the orthogonal folding of the chains into SCPNs with distinct hydrophobic compartments consisting of dodecyl and benzyl grafts respectively, as analyzed via SAXS and TEM. The folded structure was locked using covalent cross-linking of the olefin pendants. Using NOE NMR, they showed that the dodecyl and benzyl grafts in water are close together, but are located in separate compartments. The small, folded structure of the SCPNs was confirmed by SEC and DLS, showing an R_H of 7.5 nm. The polymers swelled in chloroform, but due to the covalent stabilization of the different compartments, they stayed intact. Hence, literature shows striking examples in which control over the folding pathway in SCPNs allows for the preparation of polymeric nanoparticles with distinct, stable, and structured hydrophobic compartments in water.

3.8. Compartmentalized nanoparticles for cellular applications

To prepare stable, folded SCPNs that can efficiently perform a function in complex environments, all the considerations for efficient SCPN folding outlined above need to be considered. This will be especially relevant when designing a system that requires the retention of a compartmentalized stable structure in the highly competitive cellular environment for applications such as drug delivery, as cellular censor, or for bio-orthogonal catalysis.[176] A recent review by Paulusse has highlighted specific requirements of SCPNs for successful application in a biological setting,[177] which include a detailed study on glucose-based SCPNs for cell targeting.[130]

Xin and coworkers developed random copolymers consisting of PEG methacrylate and a sextuple self-complementary hydrogen-bonding motif.[178] In water, these polymers folded into nanoparticles with controlled size with $R_H = 25$ nm as determined by DLS *via* association of the hydrogen-bonding motif. The obtained size stayed constant up to high concentrations of 40 mg mL^{-1}, indicating good size stability of the nanoparticles. Intriguingly, the nanoparticles show excellent stability in aqueous solutions containing the surfactant SDS, showing resistance to unfolding even after 48 hours, which makes them promising for applications in competitive environments such as cells, where unfolding and exposure of the hydrophobic compartments is undesirable.

We have recently published a systematic study on how SCPN structure modulates stability in complex aqueous media.[179] A library of amphiphilic random copolymers incorporating different amounts of the hydrophilic polyether Jeffamine@M1000, hydrophobic dodecyl, and/or the structuring supramolecular graft BTA, as well as the fluorescent probe Nile Red was prepared (**P2**–**P6**), see Figure 12A. In water, all polymer chains form SCPNs *via* hydrophobic and/or supramolecular interactions with an average size of $R_H = 5$–7 nm, depending on

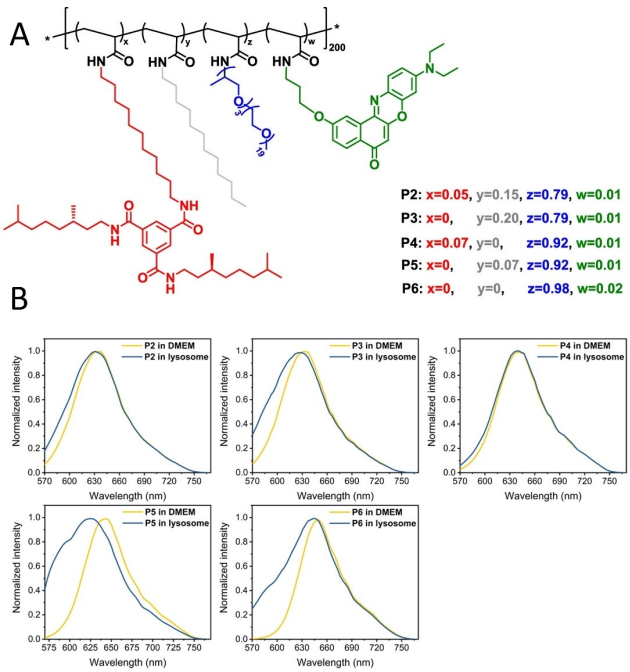

Figure 12. A) Chemical structures of amphiphilic heterograft random copolymers consisting of Jeffamine@M1000, dodecylamine, Nile Red-amine, and BTA-amine sidechains. B) Corresponding fluorescence spectra of the different copolymers in DMEM or in the lysosome of HeLa cells. Polymers lacking BTA-amine (**P3**, **P5**, and **P6**) show considerable blueshifts in lysosome compared to DMEM, whereas **P2** and **P4** show similar fluorescence in both environments, highlighting their structural stability. Image adapted from Ref. [179] licensed under CC BY-NC 3.0.

the exact polymer design. The Nile Red emission spectra revealed that all polymers **P2**–**P6** form hydrophobic compartments in water, as inferred from a blueshift in the emission maximum of Nile Red compared to pure water. However, the Nile Red fluorescence spectrum depended on the microstructure of the polymer, as the blueshift was more pronounced for polymers with more hydrophobic grafts. When introduced into complex environments, such fluorescence shifts can be used to determine interactions between the SCPNs and their environment. Regardless of polymer design, and thus the exact folded structure, all SCPNs were stable in the complex media PBS, DMEM, and DMEM supplemented with 10 vol% FBS. Good structural stability of the SCPNs was observed in the cytoplasm of HeLa cells. However, in the lysosomes, only those polymers which comprised additional stabilization via the self-assembly of incorporated BTA grafts showed sufficient structural stability, see Figure 12B. Hence, supramolecular self-assembly can protect the structural integrity of the hydrophobic compartments and shield Nile Red from unwanted cell interactions.

Additionally, control over the polymer architecture and connectivity between the functional moieties and the SCPN can modulate cell-SCPN interactions. In another study, we prepared random amphiphilic copolymers consisting of hydrophilic poly(ethylene glycol) grafts and hydrophobic dodecyl grafts that fold into SCPNS in water *via* the hydrophobic effect, and additionally incorporated functional pyrazoline moieties, see Figure 13.[180] In this study, the pyrazoline moiety was either physically encapsulated as free adduct, connected to the polymer backbone on one end as a dangling chain, or connected to the polymer backbone on both ends, acting as a cross-linker. The pyrazoline acted as a fluorescent, solvatochromic probe and reported on local interactions between the probe and its microenvironment. Regardless of polymer design, the pyrazoline fluorescence was stable and showed no shift in DMEM supplemented with 10 vol% FBS, corroborating excellent operational and conformational stability in complex media. Importantly however, upon internalization of the different polymers in HeLa cells after incubation for 24 hours, differences between the polymer architectures were observed. SCPNs with cross-linked pyrazoline moieties revealed good functional stability. However, a blueshift was observed for the pyrazoline dangling chains and an even larger shift for the free adduct, indicating an increased interaction between cellular components and the pyrazoline moiety as the connectivity of the pyrazoline to the SCPN decreased. Thus, for high functional stability in cellular environments, the polymer architecture is crucial in preventing unwanted interactions which can lead to loss of properties.

3.9. Characterization of compartmentalized structures

Similar to protein characterization, there are many techniques to characterize SCPNs.[3,5,8] ^{1}H-NMR is routinely used to follow monomer conversion and incorporation ratios. ^{1}H-NMR is quite accurate for small polymers, but for high molecular weight polymers, especially when incorporating diverse grafts, determination of the polymer length and monomer ratios becomes less accurate. Our group applies post-polymerization functionalization of pentafluorophenylacrylates with amine-functional grafts following Theato's work,[181] to introduce different types of grafts. The amide formation can be accurately followed using ^{19}F-NMR.[182] Folding or collapse of polymer chains into SCPNs should result in a decrease in average size of the polymers. SEC is used to determine the apparent molecular weight and molar mass dispersity of the polymers.[142,183,184] After SCPN formation,

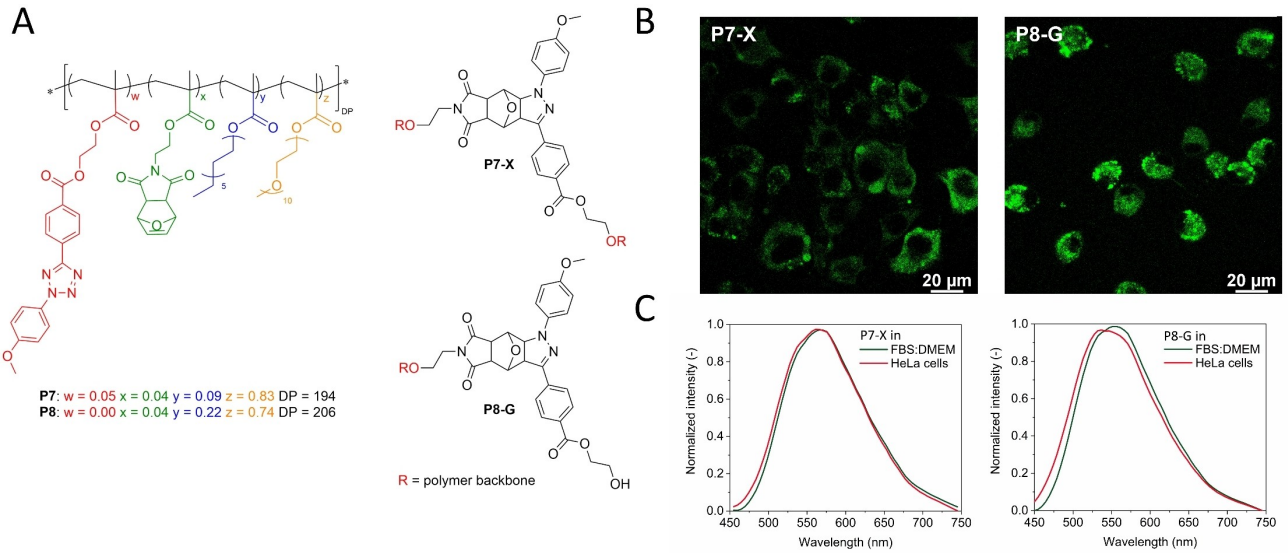

Figure 13. A) Chemical structures of polyacrylate-based random copolymers of poly(ethylene glycol) methacrylate and dodecyl methacrylate. **P8** contains furan-protected maleimide grafts, and **P7** additionally contains tetrazole grafts. Upon photoirradiation of **P7**, pyrazoline cross-links are formed (**P7-X**), whereas **P8** forms pyrazoline grafts (**P8-G**). B) Confocal microscopy images of **P7-X** and **P8-G** after incubation with HeLa cells and C) the corresponding fluorescence spectra, showing a small but pronounced blueshift for **P8-G** in HeLa cells compared to FBS:DMEM medium, whereas such a shift is not observed for **P7-X**. Image adapted from Ref. [180] licensed under CC BY-NC 3.0.

the apparent molecular weight should decrease.[167] Larger shifts then correspond to more collapsed states. A disadvantage of this technique is that relative shifts are obtained, and the true molecular weight or size of the polymer remains unknown. Both atomic force microscopy (AFM)[170] and transmission electron microscopy (TEM) can be used to visualize polymer chains and calculate approximate sizes and size distributions, although drying effects can almost never be neglected. Routine staining in TEM can also induce changes to the polymer conformation. To circumvent this, cryo-TEM can be used in select solvents, in which a very thin layer of solution is cryogenically frozen and analyzed without further modification. Scattering techniques allow for the determination of particle sizes in solution in the native state. Dynamic light scattering (DLS) is used to determine the apparent hydrodynamic radius (R_H) of the SCPNs *via* the diffusion coefficient determined from the time-dependence of the scattered light.[144] Upon SCPN formation, R_H should decrease. R_H can also be obtained *via* diffusion-ordered spectroscopy (DOSY) NMR in the same way.[131,170,185,186] Multi-angle light scattering (MALS), also known as static light scattering (SLS), and small-angle X-ray (SAXS) or neutron scattering (SANS) can be used to determine the radius of gyration (R_G) of the particles in solutions,[142] as well as the absolute molecular weight (M_W) by absolute scale fitting.[144,160,183] These are therefore the few techniques that can be used to unequivocally prove whether SCPNs consist of single or multiple polymer chains per particle.[15] Accurate determination of size and mass requires careful removal of dust, as its presence skews the obtained R_G and M_W. Using these techniques, the shape factor $\varrho = R_G/R_H$ can be calculated, which is a measure of the shape and compactness of the SCPNs. In the compact sphere limit, a factor of 0.77 is obtained, which increases for less compact or more asymmetrical particles. Multi-angle SLS will show an angular dependence for larger nanoparticles (>20 nm), which gives information on nanoparticle shape. The angular dependence of SAXS and SANS can also give shape information for particles smaller than 20 nm. By measuring over a wide range of angles, the form factor of the nanoparticles can be obtained, which describes the size and shape of the particles in detail. By fitting the obtained form factor, (changes in) the dimension, shape, and structure of the SCPNs can be determined.[15] Important to note is that different techniques determine different sizes for the same particle. This has led to large differences in the reported size trends for polymers of different masses, as outlined in a review by Barner-Kowollik *et al.*[16] Hence, care must always be taken when interpreting the results obtained by a single method, and corroborating trends with a combination of multiple methods is advised.

The presence of structured chiral compartments in aqueous SCPNs can be determined using CD spectroscopy. Examples include the self-assembly of 1,3,5-tricarboxamides (BTAs),[14] β-sheet formation,[158] or polypeptoids into helical structures.[150,187] The formation of hydrophobic compartments without discernable (chiral) structure can be carried out by NMR spectroscopy, which can show that hydrophobic protons are in a restricted environment compared to the hydrophilic protons. We recently did this for poly(acrylamide) based SCPNs with hydrophobic BTA, coumarin, and dodecyl grafts. The proton signals corresponding to these moieties were clearly visible in the good solvent $CDCl_3$, but not in D_2O. This indicates that in water, the hydrophobic grafts experience a restricted, confined environment.[175] ^{1}H-NMR is also useful to quantify the spin-spin relaxation time (T2) of open and collapsed polymer chain conformations. It was found that T2 of hydrophobic segments decreases upon polymer collapse, indicating a restriction of the mobility, and hereby molecular flexibility.[188] Alternatively, hydrophobic solvatochromic dyes can be used, which are dyes with absorbance or fluorescence properties that change depending on the polarity or mobility of their environment. Localization of the dyes inside a hydrophobic compartment results in typical absorbance or fluorescence maxima shifts or changes in fluorescence intensity.[189] Examples of such dyes include Nile Red,[179,190] 1,8-ANS,[150] and pyrene.[137] Using FRET pairs attached to the same polymer chain can show intramolecular collapse.[19,149] Alternatively, functionalizing different polymer chains with only one of the two fluorophores and preparing mixed solutions can reveal the formation of multichain aggregates.

A more recent addition to the repertoire of SCPN characterization is the use of continuous wave electron paramagnetic resonance (CW EPR).[191–194] Here, the attachment of a TEMPO spin label to the SCPN backbone can elucidate not only its compartmentalized nature, but also the effect of temperature on the mobility within the nanocompartments. In combination with Overhauser dynamic nuclear polarization,[191] information on the local water translational diffusion dynamics around the spin label can be gained. The latter may help to understand why some SCPN structures provide better catalyst carriers than others.

Recently, the heterogeneity of SCPNs using super resolution microscopy was analyzed.[195] By surface immobilization of amphiphilic random copolymers with the dye Nile Red covalently attached, the spectral point accumulation for imaging in nanoscale topography (NR-sPAINT) technique could be applied. This super-resolution fluorescence technique revealed the polarity of the hydrophobic compartments of SCPNs at the single molecule level, see Figure 14. Polymer designs with increasing hydrophobic/hydrophilic ratio showed a clear shift in polarity. Moreover, not only was a remarkable heterogeneity in polarity observed between particles of the same polymer design, but also within one particle, highlighting that polymer synthesis leads to ensembles of particles with unique, varied properties.

3.10. From structure to function

Many different application areas have been evaluated for SCPNs including drug carrier systems,[17,177] bio-orthogonal catalysts,[17,28,196] sensors,[196] and contrast and cell imaging agents.[177] The polymer design is guided by the envisioned application area, as each application demands specific properties. The beauty of this approach towards functional nano-

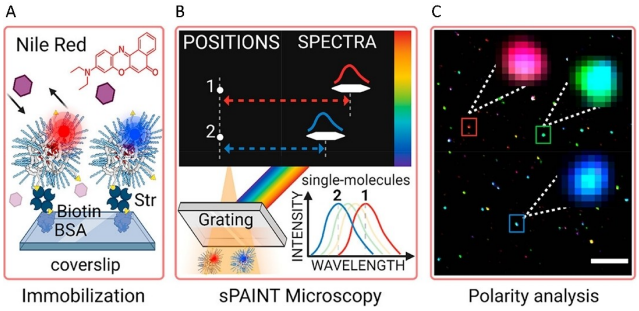

Figure 14. A) Amphiphilic random copolymers that fold into SCPNs in water are immobilized on a glass surface in the presence of Nile Red. B) NR-sPAINT is used to simultaneously record the position as well as the emission spectrum of NR located within individual SCPNs. C) Analysis of individual emission events allows for the polarity analysis to assess structural heterogeneity within a single SCPN and between multiple SCPNs. Image reprinted from Ref. [195] licensed under CC BY 4.0.

particles is that a single polymer chain, through proper monomer or graft design, can fold into a nanoparticle with a specific function. Formation of one, or multiple,[144] internal hydrophobic pockets provides a segregated environment for protection of "cargo" to establish new function and protect or shield it in otherwise hostile environments, or alternatively protect the environment from otherwise hostile "cargo". Over the years multiple approaches to design such systems have been put forward, and here we will highlight some interesting examples in different application areas.

3.10.1. Green and bio-orthogonal catalysis

Many types of polymeric nanoreactors for green catalysis have been studied, such as dendrimers, polymersomes, and micelles,[28,197] or microgel star polymers.[198,199] Single-chain polymeric nanoparticles are an attractive alternative, as the formation of structured hydrophobic nanocompartments provides a selective reaction space for catalysts. Excellent reviews deal with the development of SCPNs for catalysis using transition metal or bio-inspired catalysts, so we here focus on examples highlighting how the polymer's microstructure affects the resulting nanoparticles performance.[196,200–202]

In an early study by Terashima *et al.*, a segmented copolymer consisting of PEG methacrylate (PEGMA), BTA methacrylate (BTAMA) and diphenylphosphinostyrene formed structured, hydrophobic compartments in water due to BTA aggregation. $RuCl_2(PPh_3)_3$, served as the polymerization catalysts but in a ligand-exchange reaction also complexed to the triphenylphosphine pendants to afford catalytically active SCPNs.[157] This ruthenium-based catalyst resulted in efficient transfer hydrogenation in water. This polymer design proved to be readily adapted to widen the reaction scope. Incorporation of L-proline as catalytic unit in a follow-up study by Huerta *et al.* effectively catalyzed asymmetric aldol reactions.[203] Importantly, the catalytic reaction only occurred when the polymers were in their folded state, and with the structured hydrophobic compartments present. A general post-functionalization modification strategy developed by Liu *et al.* allowed for a modular synthesis of catalytically active SCPNs with different functionalities. Random copolymers that fold into SCPNs were designed to carry out aqueous catalysis by incorporating either Cu(I) or Pd(II) transition metal catalysts (TMCs), which effectively catalyzed azide-alkyne cycloadditions and depropargylation reactions in PBS, respectively.[182] Alternatively, incorporating porphyrin as photosensitizer resulted in singlet oxygen generation upon photoirradiation, which successfully released a pro-drug attached to the polymers via a singlet oxygen-cleavable aminoacrylate linker. In a follow-up work, the biocompatible SCPNs were selectively localized in different cellular compartments and bio-orthogonal catalysis was performed.[204] The Cu(I)- and Pd(II)-decorated SCPNs both performed carbamate cleavage reactions to deprotect rhodamine-based dyes, which acted as model substrate for pro-drug activation. Additionally, the porphyrin-decorated SCPNs successfully produced singlet oxygen upon photoirradiation, inducing cell death, showing potential for anti-cancer therapy. These initial studies were followed by a systematic study by Sathyan *et al.* Herein, the crucial parameters were identified that determined the efficiency and stability of catalytically active Pd(II)-decorated polymeric nanoparticles (Figure 15A) when going from water or PBS to DMEM, a biologically relevant medium.[205] The catalytic activity in water was primarily impacted by the different metal-ligand complexes used, and less so by the polymer microstructure. The concentrator effect, in which hydrophobic substrates feel a driving force towards hydrophobic compartments in water, allowed for efficient catalysis even at low catalyst and substrate loading, and more hydrophobic substrates reacted faster. In water, the rate of a physically entrapped Pd(II) complex (**P9**) was similar to Pd(II) complexed to a covalently attached triphenylphosphine ligand (**P10**–**P11**). However, in DMEM, ligand attachment was crucial to retain the activity of the SCPNs, such as for the deprotection of pro-rhodamine (Figure 15B). Increasing the system's complexity by providing better stabilization of the metal *via* a structured interior as in **P11**, resulted in a small increase in catalytic activity compared to **P10** with an unstructured interior. Different anti-cancer pro-drugs such as 5-FU, paclitaxel, or doxorubicin were also activated in DMEM, albeit at a slower rate than in water.

The group of Zimmerman conducted a series of in-depth studies to achieve fast catalytic conversions in biological media. Chen *et al.* designed Cu(I) containing random copolymers that fold into SCPNs in PBS with different water-solubilizing graft, being cationic, anionic, zwitterionic, or neutral in nature.[133] More hydrophobic substrates were catalyzed more efficiently, highlighting the importance of the concentrator effect. Importantly, substrates with complementary charge to the water-solubilizing grafts were catalyzed at a higher rate as well, while those with opposite charge were catalyzed less, showing that both hydrophobicity and charge-complementarity play a role in the concentrator effect, see Figure 16. In a recent study, Garcia *et al.* synthesized Ru-containing SCPNs that catalyzed the cleavage of allylcarbamate groups in PBS and DMEM.[206] However, the substrate conversion was decreased from 60 to 30% when going from PBS to DMEM, and the reaction rate

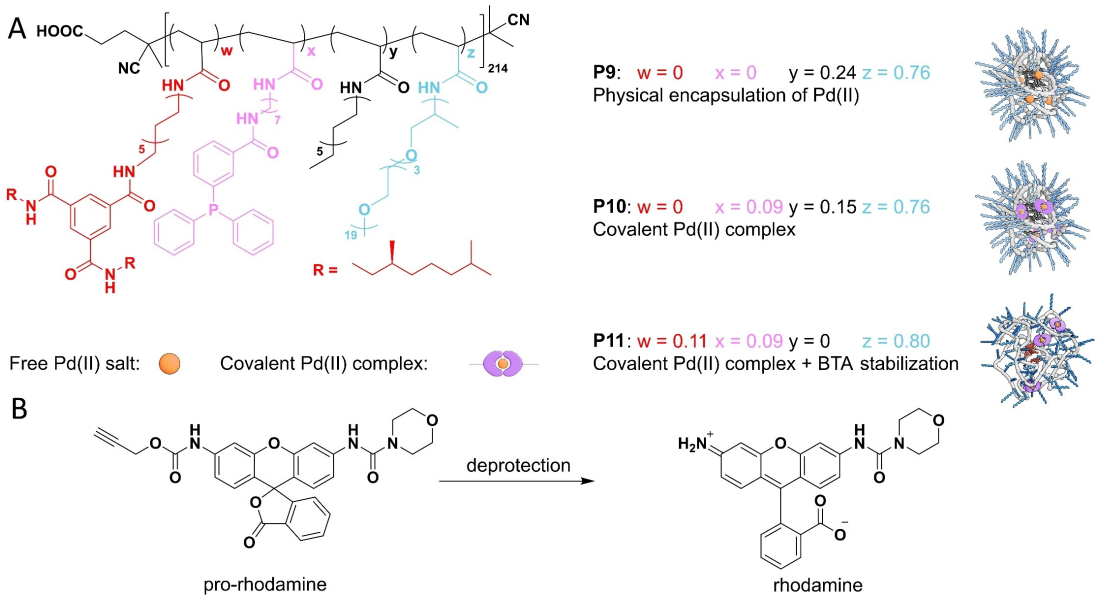

Figure 15. A) Chemical structure of heterograft random copolymers that fold into polymeric nanoparticles in water *via* hydrophobic collapse. Pd(II) is physically encapsulated as Pd(II) salt in **P9**, or covalently attached as a Pd(II)-phosphine complex in **P10** and **P11**. **P11** incorporates additional stability *via* the self-assembly of BTA grafts. B) The metal-catalyzed deprotection of pro-rhodamine proceeds *via* the catalytically active nanoparticles.

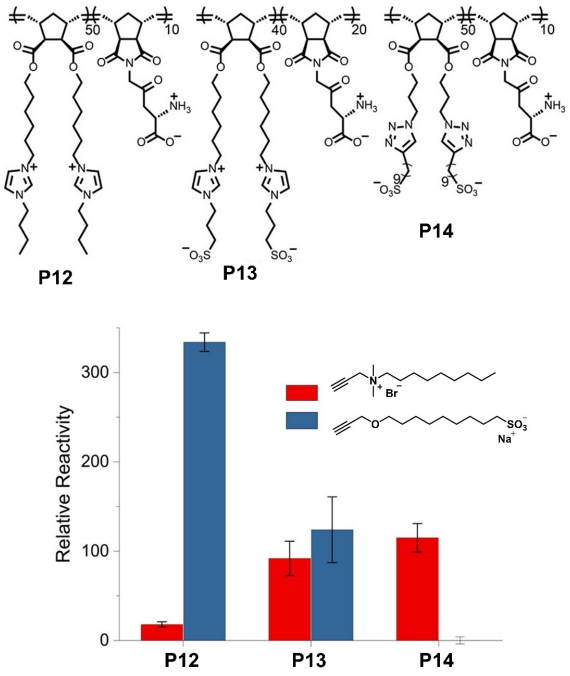

Figure 16. Chemical structures of random copolymers prepared via ROMP and a subsequent post-functionalization approach to prepare cationic (**P12**), zwitterionic (**P13**), or anionic (**P14**) copolymers (top). The relative reactivity of a positively (red) and negatively (blue) charged substrate for the three polymers (bottom). Adapted with permission from Ref. [133]. Copyright 2018 American Chemical Society.

decreased 3-fold as well, indicating that structural improvements to the SCPN are still desired. The cleaved product further functioned as substrate in a tandem reaction with β-gal to release the fluorescent dye coumarin 7, acting as proof-of-concept for prodrug activation strategies.

Chen *et al.* introduced their Cu(I) containing random copolymers to HeLa cells.[207] SCPNs decorated with ammonium-presenting water solubilizing groups readily perform azide-alkyne cycloadditions on alkynated proteins and small substrates, but also interacted with cellular membranes. When PEG grafts were employed instead, interactions with proteins were shielded, and only small substrates were converted. Coincidently, this PEG shell also resisted cellular uptake of the SCPNs. Hence, the PEG-decorated SCPNs could be used for extracellular click reactions on small substrates, which in turn diffused into the HeLa cells. Additionally, the ammonium-presenting water solubilized SCPNs functionalized with Ru-catalysts complexed to proteins such as β-gal, and acted as transportation vehicles to codeliver β-gal into endosomes, see Figure 17.[208] The SCPNs and β-gal showed concurrent deprotection of prodrugs, resulting in a decrease of cell viability. This strategy also allowed for bio-orthogonal tandem reactions between the SCPN and enzymes. As model reaction, a coumarin coupled to an azido phenyl carbonate protected-galactose unit was used as substrate for tandem catalysis in cells. First, the galactose was deprotected via Ru-mediated azido phenyl carbonate cleavage, upon which β-gal cleaved the galactose from the coumarin, releasing the fluorescent dye. Once again, unwanted interactions between SCPNs and cellular components resulted in a decrease in activity, highlighting the importance of structural control in SCPN design to retain function. As a final illustration of bio-orthogonal catalysis, Huang *et al.* designed water-soluble cationic SCPNs loaded with hydrophobic Fe-catalysts.[209] The catalytic SCPNs were incorporated into bacterial biofilms, where the positive charge aided biofilm penetration. The Fe-catalysts deprotected the aryl-azide carbamate protected antimicrobial prodrugs pro-moxifloxacin and pro-ciprofloxacin, resulting in biofilm degradation.

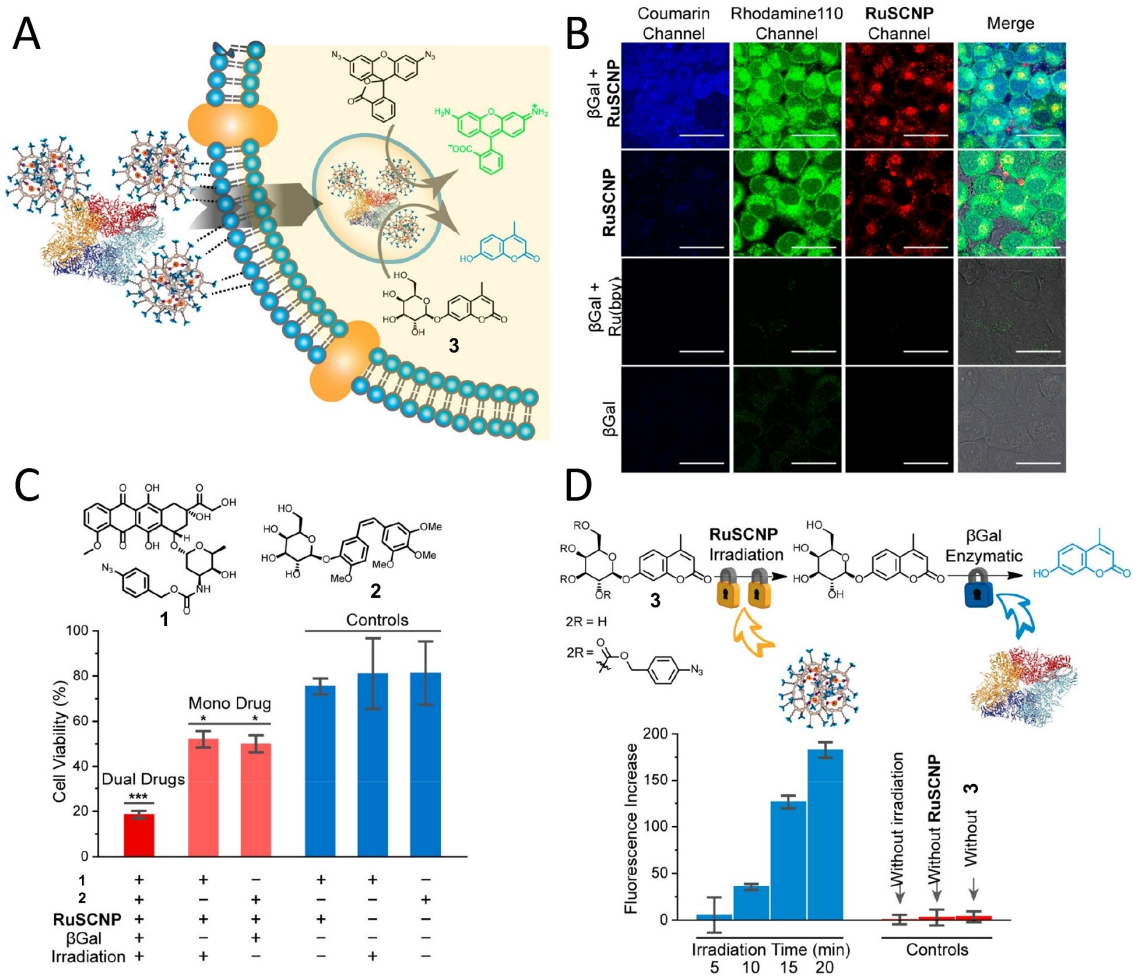

Figure 17. A) Random heterograft copolymers are decorated with ammonium groups, allowing them to complex to proteins such as β-gal, and codeliver them into endosomes. B) Confocal microscopy imaging showing successful deprotection of pro-coumarin by β-gal inside cells after codelivery *via* SCPNs, as well as deprotection of pro-rhodamine110 by the Ru-functionalized SCPNs. C) Concurrent deprotection of model drugs by the Ru-functionalized SCPN and β-gal results in higher cell death than deprotection of only one drug. D) Tandem deprotection of a protected-galactose coupled to coumarin by the Ru-functionalized SCPN and subsequent cleavage of the galactose by β-gal results in successful release of coumarin in cells. Adapted with permission from Ref. [208]. Copyright 2020 American Chemical Society.

3.10.2. MRI contrast agents

SCPNs have also been investigated by Perez-Baena *et al.* as potential MRI contrast agents.[210] A random copolymer based on PEGMA was cross-linked to drive polymer collapse, see Figure 18. The cross-linker contained Gd(III) complexing ligands, a metal used as MRI contrast agent. Importantly, after complexation, the resulting water-soluble SCPNs contained rigid, paramagnetic Gd(III) centers that showed a 2-fold increased relaxivity compared to the often-used contrast agent Magnevist®, displaying the high potential of this approach.

3.10.3. Cellular targeting

SCPNs have also been investigated for targeted imaging or drug-delivery in cells, where either specific compartments of an organism, or specific compartments inside a cell are selectively targeted for visualization or treatment with drugs, with an excellent review having been written by Kröger *et al.*[177] Here we highlight a few diverse examples to capture the breadth in potential application areas. Kröger *et al.* synthesized a series of random copolymers consisting of xanthate methacrylate and glucose methacrylate.[130] The glucose moieties were conjugated to the polymer backbone either at the C1 or C6 position, or with methyl glucoside conjugated at the C6 position as well. The polymers were folded into SCPNs through cross-linking of thiol-functional grafts after deprotection of the xanthate using hydrazine. The resulting nanoparticles were taken up by HeLa cells via endocytosis and localized primarily within late endosomes and lysosomes, which therefore shows potential for tumor targeting. Importantly, the glucose conjugation position determined the uptake efficiency within the HeLa cells, with C6 conjugation resulting in highest uptake, and C1 conjugation the lowest. The methyl glucoside conjugated at the C6 position was taken up to an intermediate amount. Hence, it was shown that subtle control over the polymer design can modulate the interactions with cells.

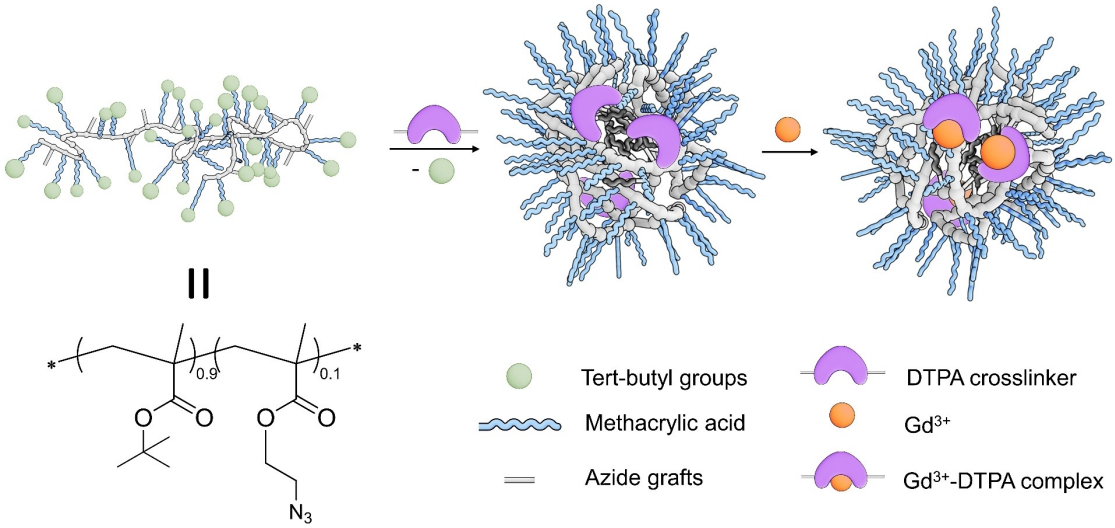

Figure 18. PEGMA-based random copolymers are collapsed into SCPNs *via* cross-linking using a bifunctional DTPA cross-linker. Subsequent functionalization with Gd(III) ions results in SCPNs with paramagnetic properties.

Hamelmann *et al.* designed SCPNs to target the ookinete stage of the malaria parasite, for which they used previously designed biocompatible random copolymers of solketal methacrylate and xanthate methacrylate.[211] To render the copolymers water-soluble, the solketal moieties were hydrolyzed to glycerol. Next, the copolymers were folded into SCPNs *via* cross-linking of deprotected xanthate moieties using thiol-Michael addition chemistry. Finally, the SCPNs were decorated with negative surface charges *via* partial decoration of the glycerol with succinate groups to endow the SCPNs with targeting properties. By feeding food mixed with SCPNs to mosquitos, the SCPNs were taken up in the midguts of the insects.[212] With an increasing amount of negative surface charge, the uptake by ookinetes increased and successful internalization was confirmed, suggesting that malaria parasites can be targeted by feeding SCPNs to mosquitoes, see Figure 19. The SCPNs were additionally covalently decorated with the anti-malarial atovaquone, although deprotection of the drug still needed to be optimized and as such, no significant inhibition of ookinete development was found yet.

Benito *et al.* set out to design SCPNs which target pancreatic cancer.[213] To this end, poly(methacrylic acid) based copolymers were synthesized and functionalized with the cancer-targeting peptide PTR86 and the radioactive isotope ^{67}Ga for visualization using SPECT imaging. Additional cross-linking afforded SCPNs with small sizes in water, see Figure 20. Upon treating tumor-bearing mice with the SCPN solution, higher retention in the tumors was found for PTR86-decorated SCPNs with respect to undecorated SCPNs, which showed lower tumor-to-muscle distribution ratios. Hence, the current SCPN design is promising for solid cancer diagnosis. Subsequent incorporation of anti-cancer drugs into the SCPNs should prove useful for the further development of SCPNs towards anti-cancer therapy.

3.10.4. Protein stabilization

Random copolymers have also been successfully used for the stabilization of proteins, in particular by the group of Xu.[25,214,215] Xu and coworkers designed random heteropolymers (RHPs) based on methacrylate monomers, being hydrophilic poly(ethylene glycol) methacrylate (PEGMA), hydrophobic methyl methacrylate (MMA) and 2-ethylhexylmethacrylate (2-EHMA), and the negatively charged 3-sulfopropyl methacrylate

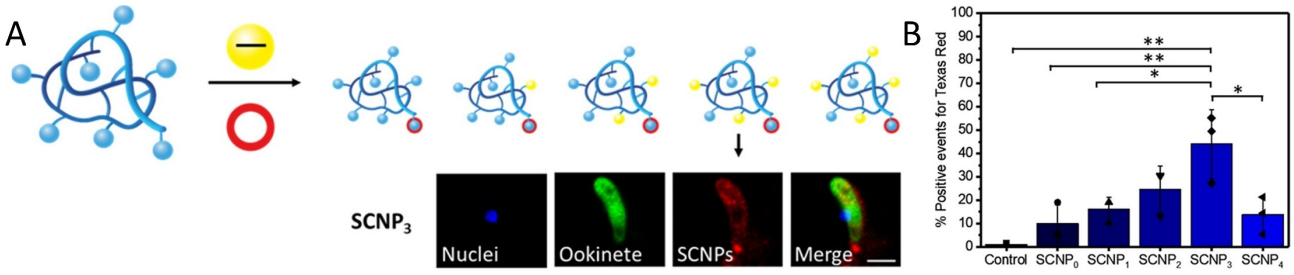

Figure 19. A) Biocompatible random copolymers are decorated with negative surface charges *via* succinate conjugation (yellow circles) and are taken up by ookinetes as measured by confocal microscopy *via* Texas Red fluorescence (red circles). The nanoparticle fluorescence overlaps with that of stained ookinetes, highlighting successful incorporation. B) The uptake by ookinetes increases with increasing negative surface charge of the polymer, from $SCNP_0$ to $SCNP_3$ (from −5 to −32 mV). Image reprinted from Ref. [212] licensed under CC BY 4.0.

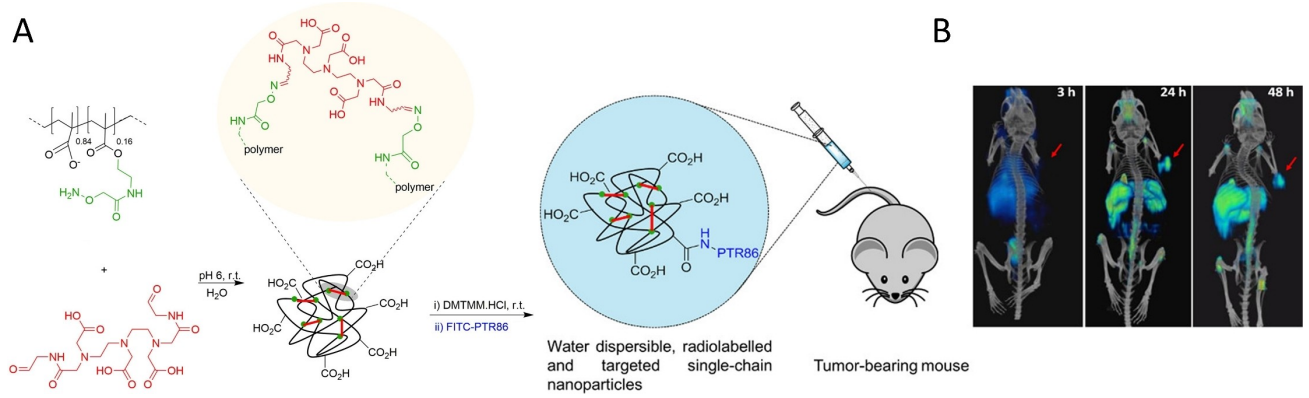

Figure 20. A) Chemical structure of poly(methacrylic acid)-based random copolymers folded into SCPNs *via* covalent cross-linking. The nanoparticles were functionalized with PTR86, a pancreatic tumor-targeting moiety, and ^{67}Ga to visualize the polymers using SPECT imaging. The SCPNs were injected into tumor-bearing mice. B) Visualization of the biodistribution of SCPNs in tumor-bearing mice after 3, 24, and 48 hours. Localization in the pancreatic tumor is observed after 24 h as indicated by the observed ^{67}Ga intensity next to the red arrow. Reprinted with permission from Ref. [213]. Copyright 2016 American Chemical Society.

potassium salt (3-SPMA) in a specific ratio to perfectly compliment the exposed hydrophilic, hydrophobic, and positively charges surfaces areas of membrane proteins, respectively, see Figure 21.[214] Complexation between either oligopeptide/proton symporter PepTso or water channel aquaporin Z (AqpZ) with the random copolymers in water occurred successfully, resulting in the proper folding and stabilization of the membrane proteins in cell-free environments. The proteins showed active proton transport after reconstitution in liposomes, highlighting that the copolymers do not interfere with the function of the proteins. In a follow-up study, random copolymers of the same four monomers in the previous study were synthesized at specific ratios promoting incorporation into lipid bilayers.[215] The random copolymers distributed themselves in the lipid bilayer, forming bilayer-spanning segments, allowing for proton transport through the bilayer. In their latest work, random copolymer mixtures with precise monomer ratios were synthesized to carry out specific functions.[25] Here, the random copolymers proved to be capable of assisting protein folding, enhancing the thermal stability of proteins, and acting as a synthetic substitute for the cytosol. In these studies, it was shown that complex, biologically relevant functions can be conducted by random copolymers without a defined primary sequence but instead consisting of a mixture of individual polymer chains only similar in their average monomer composition.

Synthetic polymers have also been applied as inhibitors of amyloid-β peptide aggregation, responsible for Alzheimer's disease.[66] Many different polymeric designs have been reported so far, relying on targeted as well as aspecific interactions to prevent or disrupt amyloid aggregation. Of particular interest is the work by Binder and coworkers, who used polymers based on poly(ethylene oxide) acrylate and different hydrophobic end-groups for a specific hydrophilic/hydrophobic ratio.[216–220] The hydrophobic end-groups were either a long aliphatic alkyl chain, or cholesteryl or diacylglyceryl moieties that can bind to the hydrophobic domains of amyloid-β, see Figure 22. This interaction between the polymers and the amyloid inhibits further binding of the amyloid-β monomers, showing an up to 10 times higher lag time for fibril

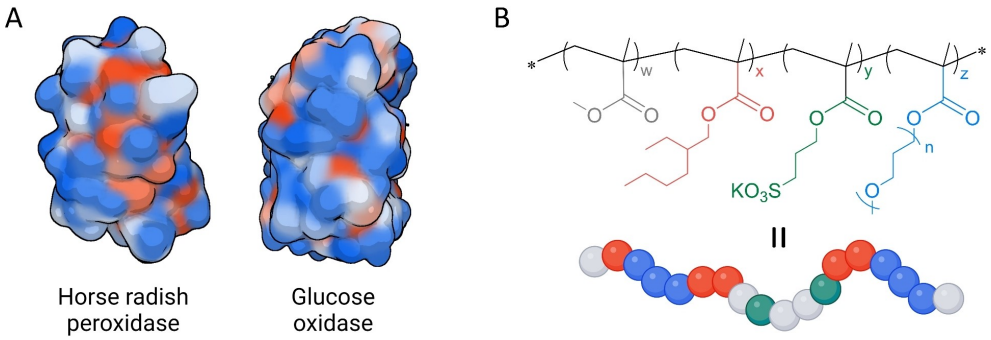

Figure 21. A) The surface hydrophilicity (hydrophilic = blue, hydrophobic = red) of horse radish peroxidase and glucose oxidase, two common proteins. B) Random heteropolymer design consisting of hydrophilic poly(ethylene glycol) methacrylate (PEGMA, blue), hydrophobic methyl methacrylate (MMA, grey) and 2-ethylhexylmethacrylate (2-EHMA, red), and the negatively charged 3-sulfopropyl methacrylate potassium salt (3-SPMA, green). By complementary design (= specific monomer ratios) of the random copolymers to the protein surface, the polymers complexed and maximized polymer-protein interactions in a complementary fashion, leading to solubilization and stabilization of the proteins in organic solvents, reducing denaturation. Image created with BioRender.com.

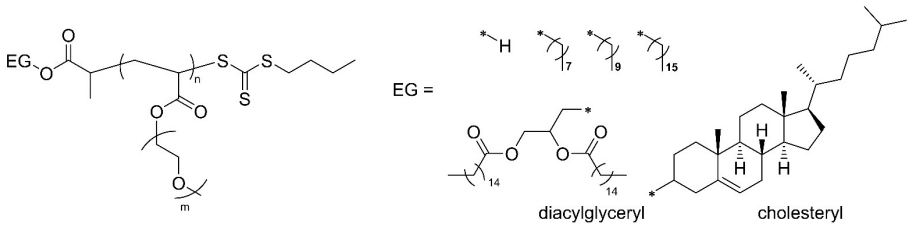

Figure 22. Chemical structure of EG_$P_n(EO)_m$A poly(ethylene oxide) acrylate polymers with degree of polymerization n and specific ethylene oxide chain length m functionalized with a hydrophobic end-groups (EG), either an aliphatic chain, or a membrane anchor: diacylglyceryl or cholesteryl.

formation in the presence of G_$P_{11}(EO)_3$A compared to uninhibited amyloid-β, hence inhibiting the formation of amyloid fibrils responsible for Alzheimer's disease.

4. Summary and Outlook

Proteins are inspiring machines for synthetic chemists to mimic due to the specific properties arising from their structure. However, the requirement for the formation of the specific 3D structure to achieve function also comes with difficulties in misfolding and aggregation, leading to loss of activity and unwanted side effects, such as disease. Synthetic systems cannot be expected to have the same properties as proteins as we strive to impart them with non-native function, but they are also fundamentally different. Proteins are translated, folded, and conduct their function *in vivo*, after which they are destroyed. Synthetic systems with biological applications on the other hand, can be prepared in the lab, need to be delivered to the desired site in the body, conduct their function at that site, without bodily regulation machinery that can modulate or control their function. They will have to be prepared exactly right and be active long enough to carry out their job. To this end, when designing synthetic polymeric systems for applications in aqueous media or biological environments, there are certain requirements for a good functioning system. We believe that smart polymer design can fulfil those demands. As we have shown, the folding of synthetic random copolymers shares key features with the folding of structurally defined proteins as well as with IDPs. Overall, we believe that the desired application should guide the polymer design. More sequence control might not always be required, or in some cases, even be desired. It is therefore always crucial to determine what level of control is needed and if the potential gain in properties is worth the cost.

While synthetic polymers are still far from mimicking proteins in their structural complexity and functionality, the formation of well-defined nanoparticles in water offers many opportunities in designing simple systems by utilizing the key principles of protein folding to impart aqueous nanoparticles with compartmentalized spaces to conduct specific functions. The strength of amphiphilic heterograft polymers lies in the potential of simple, synthetically accessible polymer design to create nanoparticles with compartmentalized structure with highly modular function for different potential applications[221] in areas such as aqueous (green) catalysis using water-incompatible catalysts, or bio-orthogonal catalysis in a shielded environment.[17,28,196] Pro-drug activation for cancer therapy, drug carriers,[17,177] sensors,[196] and imaging in living organisms through fluorescence or as MRI contrast agents are other potential application areas.[177] As Connal said in a recent review on enzyme-inspired synthetic hydrolytic catalysts: *"incorporating the design principles laid down by nature will be a surefire way forward"*.[28] Taking inspiration from the folding of proteins in nature and the way nature derives function through structure is a highly promising way towards the development of synthetic nanoparticles that can contribute towards solving the challenges of today.

Acknowledgements

The authors acknowledge funding by the Dutch Ministry of Education, Culture and Science (Gravity Program 024.001.035). The ICMS Animation Studio (Eindhoven University of Technology) is acknowledged for providing artwork.

Conflict of Interests

The authors declare no conflict of interest.

Data Availability Statement

Data sharing is not applicable to this article as no new data were created or analyzed in this study.

Keywords: protein folding · nanocompartments · nanoparticles · self-assembly · synthetic polymers

[1] H. Staudinger, *Ber. Dtsch. Chem. Ges. A* **1920**, *53*, 1073–1085.
[2] M. A. M. Alqarni, C. Waldron, G. Yilmaz, C. R. Becer, *Macromol. Rapid Commun.* **2021**, *42*, 1–17.
[3] J. A. Pomposo, Ed., *Single-Chain Polymer Nanoparticles: Synthesis, Characterization, Simulations and Applications*, Wiley-VCH, Weinheim, **2017**.
[4] E. Verde-Sesto, A. Blázquez-Martín, J. A. Pomposo, *Polymer* **2019**, *11*, 1903–1923.
[5] M. Huo, N. Wang, T. Fang, M. Sun, Y. Wei, J. Yuan, *Polymer* **2015**, *66*, A11–A21.

[6] A. Sanchez-Sanchez, I. Pérez-Baena, J. A. Pomposo, *Molecules* **2013**, *18*, 3339–3355.
[7] O. Altintas, C. Barner-Kowollik, *Macromol. Rapid Commun.* **2016**, *37*, 29–46.
[8] C. K. Lyon, A. Prasher, A. M. Hanlon, B. T. Tuten, C. A. Tooley, P. G. Frank, E. B. Berda, *Polym. Chem.* **2015**, *6*, 181–197.
[9] J.-F. Lutz, J.-M. Lehn, E. W. Meijer, K. Matyjaszewski, *Nat. Rev. Mater.* **2016**, *1*, 16024.
[10] M. Rohmer, J. Freudenberg, W. H. Binder, *Macromol. Biosci.* **2023**, *23*, 2200344.
[11] J. H. Ko, H. D. Maynard, *Chem. Soc. Rev.* **2018**, *47*, 8998–9014.
[12] H. A. Klok, *Macromolecules* **2009**, *42*, 7990–8000.
[13] G. M. ter Huurne, A. R. A. Palmans, E. W. Meijer, *CCS Chem.* **2019**, *1*, 64–82.
[14] P. J. M. Stals, M. A. J. Gillissen, T. F. E. Paffen, T. F. A. De Greef, P. Lindner, E. W. Meijer, A. R. A. Palmans, I. K. Voets, *Macromolecules* **2014**, *47*, 2947–2954.
[15] M. A. J. Gillissen, T. Terashima, E. W. Meijer, A. R. A. Palmans, I. K. Voets, *Macromolecules* **2013**, *46*, 4120–4125.
[16] E. Blasco, B. T. Tuten, H. Frisch, A. Lederer, C. Barner-Kowollik, *Polym. Chem.* **2017**, *8*, 5845–5851.
[17] J. A. Pomposo, *Polym. Int.* **2014**, *63*, 589–592.
[18] Y. Morishima, S. Nomura, T. Ikeda, M. Seki, M. Kamachi, *Macromolecules* **1995**, *28*, 2874–2881.
[19] S. Yusa, A. Sakakibara, T. Yamamoto, Y. Morishima, *Macromolecules* **2002**, *35*, 10182–10188.
[20] G. Njikang, G. Liu, L. Hong, *Langmuir* **2011**, *27*, 7176–7184.
[21] J. De–La-Cuesta, E. González, J. Pomposo, *Molecules* **2017**, *22*, 1819–1832.
[22] Y. Bai, X. Feng, H. Xing, Y. Xu, B. K. Kim, N. Baig, T. Zhou, A. A. Gewirth, Y. Lu, E. Oldfield, S. C. Zimmerman, *J. Am. Chem. Soc.* **2016**, *138*, 11077–11080.
[23] M. Collot, J. Schild, K. T. Fam, R. Bouchaala, A. S. Klymchenko, *ACS Nano* **2020**, *14*, 13924–13937.
[24] Z. Han, S. L. Hilburg, A. Alexander-Katz, *Macromolecules* **2022**, *55*, 1295–1309.
[25] Z. Ruan, S. Li, A. Grigoropoulos, H. Amiri, S. L. Hilburg, H. Chen, I. Jayapurna, T. Jiang, Z. Gu, A. Alexander-Katz, C. Bustamante, H. Huang, T. Xu, *Nature* **2023**, *615*, 251–258.
[26] C. Nagao, M. Sawamoto, T. Terashima, *J. Polym. Sci.* **2020**, *58*, 215–224.
[27] M. H. Barbee, Z. M. Wright, B. P. Allen, H. F. Taylor, E. F. Patteson, A. S. Knight, *Macromolecules* **2021**, *54*, 3585–3612.
[28] M. D. Nothling, Z. Xiao, A. Bhaskaran, M. T. Blyth, C. W. Bennett, M. L. Coote, L. A. Connal, *ACS Catal.* **2019**, *9*, 168–187.
[29] J. De Neve, J. J. Haven, L. Maes, T. Junkers, *Polym. Chem.* **2018**, *9*, 4692–4705.
[30] J.-F. Lutz, *Macromol. Rapid Commun.* **2017**, *38*, 1700582.
[31] B. A. F. Le Bailly, J. Clayden, *Chem. Commun.* **2016**, *52*, 4852–4863.
[32] G. Guichard, I. Huc, *Chem. Commun.* **2011**, *47*, 5933.
[33] A. Nitti, R. Carfora, G. Assanelli, M. Notari, D. Pasini, *ACS Appl. Nano Mater.* **2022**, *5*, 13985–13997.
[34] L. Li, K. Raghupathi, C. Song, P. Prasad, S. Thayumanavan, *Chem. Commun.* **2014**, *50*, 13417–13432.
[35] M. Sela, F. H. White, C. B. Anfinsen, *Science* **1957**, *125*, 691–692.
[36] C. B. Anfinsen, E. Haber, M. Sela, F. H. White, *Proc. Natl. Acad. Sci. USA* **1961**, *47*, 1309–1314.
[37] E. Haber, C. B. Anfinsen, *J. Biol. Chem.* **1962**, *237*, 1839–1844.
[38] C. B. Anfinsen, *Science* **1973**, *181*, 223–230.
[39] K. A. Dill, *Protein Sci.* **1999**, *8*, 1166–1180.
[40] K. A. Dill, J. L. MacCallum, *Science* **2012**, *338*, 1042–1046.
[41] K. A. Dill, *Biochemistry* **1990**, *29*, 7133–7155.
[42] K. A. Dill, S. Bromberg, K. Yue, H. S. Chan, K. M. Ftebig, D. P. Yee, P. D. Thomas, *Protein Sci.* **2008**, *4*, 561–602.
[43] R. E. Hubbard, M. Kamran Haider, *eLS* **2010**, DOI 10.1002/9780470015902.a0003011.pub2.
[44] A. Nicholls, K. A. Sharp, B. Honig, *Proteins Struct. Funct. Genet.* **1991**, *11*, 281–296.
[45] A. Zarrine-Afsar, S. Wallin, A. M. Neculai, P. Neudecker, P. L. Howell, A. R. Davidson, S. C. Hue, *Proc. Natl. Acad. Sci. USA* **2008**, *105*, 9999–10004.
[46] C. Levinthal, *J. Chim. Phys.* **1968**, *65*, 44–45.
[47] R. Zwanzig, A. Szabo, B. Bagchi, *Proc. Nat. Acad. Sci.* **1992**, *89*, 20–22.
[48] V. I. Abkevich, A. M. Gutin, E. I. Shakhnovich, *Biochemistry* **1994**, *33*, 10026–10036.
[49] P. Mishra, S. K. Jha, *Biophys. Chem.* **2022**, *283*, 106761.
[50] D. J. Brockwell, S. E. Radford, *Curr. Opin. Struct. Biol.* **2007**, *17*, 30–37.
[51] A. Šali, E. Shakhnovich, M. Karplus, *Nature* **1994**, *369*, 248–251.
[52] M. Karplus, *Folding Des.* **1997**, *2*, S69–S75.
[53] S. Bhatia, J. B. Udgaonkar, *Chem. Rev.* **2022**, *122*, 8911–8935.
[54] G. Rajpal, P. Arvan, in *Handb. Biol. Act. Pept.*, Elsevier, **2013**, pp. 1721–1729.
[55] P. J. Hogg, *Trends Biochem. Sci.* **2003**, *28*, 210–214.
[56] M. Arai, K. Kuwajima, in *Advances*, **2000**, pp. 209–282.
[57] J. Jumper, R. Evans, A. Pritzel, T. Green, M. Figurnov, O. Ronneberger, K. Tunyasuvunakool, R. Bates, A. Žídek, A. Potapenko, A. Bridgland, C. Meyer, S. A. A. Kohl, A. J. Ballard, A. Cowie, B. Romera-Paredes, S. Nikolov, R. Jain, J. Adler, T. Back, S. Petersen, D. Reiman, E. Clancy, M. Zielinski, M. Steinegger, M. Pacholska, T. Berghammer, S. Bodenstein, D. Silver, O. Vinyals, A. W. Senior, K. Kavukcuoglu, P. Kohli, D. Hassabis, *Nature* **2021**, *596*, 583–589.
[58] U. Adhikari, B. Mostofian, J. Copperman, S. R. Subramanian, A. A. Petersen, D. M. Zuckerman, *J. Am. Chem. Soc.* **2019**, *141*, 6519–6526.
[59] K. W. Plaxco, K. T. Simons, D. Baker, *J. Mol. Biol.* **1998**, *277*, 985–994.
[60] K. Lindorff-Larsen, S. Piana, R. O. Dror, D. E. Shaw, *Science* **2011**, *334*, 517–520.
[61] D. Baker, *Protein Sci.* **2019**, *28*, 678–683.
[62] D. Balchin, M. Hayer-Hartl, F. U. Hartl, *Science* **2016**, *353*, aac4354.
[63] A. R. Dinner, A. Šali, L. J. Smith, C. M. Dobson, M. Karplus, *Trends Biochem. Sci.* **2000**, *25*, 331–339.
[64] I. Kuznetsova, K. Turoverov, V. Uversky, *Int. J. Mol. Sci.* **2014**, *15*, 23090–23140.
[65] C. M. Dobson, *Nature* **2003**, *426*, 884–890.
[66] Rupali, B. Joseph, S. Thomas, N. Sen, A. Paschold, W. H. Binder, S. Kumar, *Polym. Chem.* **2023**, *14*, 392–411.
[67] K. Araki, N. Yagi, K. Aoyama, C.-J. Choong, H. Hayakawa, H. Fujimura, Y. Nagai, Y. Goto, H. Mochizuki, *Proc. Nat. Acad. Sci.* **2019**, *116*, 17963–17969.
[68] L. Marzban, *Exp. Gerontol.* **2003**, *38*, 347–351.
[69] S. B. Prusiner, *Proc. Nat. Acad. Sci.* **1998**, *95*, 13363–13383.
[70] S. B. Prusiner, *Science* **1982**, *216*, 136–144.
[71] E. Rennella, G. J. Morgan, N. Yan, J. W. Kelly, L. E. Kay, *J. Am. Chem. Soc.* **2019**, *141*, 13562–13571.
[72] A. K. Buell, *Chem. Sci.* **2022**, *13*, 10177–10192.
[73] A. Deiana, S. Forcelloni, A. Porrello, A. Giansanti, *PLoS One* **2019**, *14*, e0217889.
[74] S. DeForte, V. N. Uversky, *RSC Adv.* **2016**, *6*, 11513–11521.
[75] T. Handa, D. Kundu, V. K. Dubey, *Int. J. Biol. Macromol.* **2023**, *224*, 243–255.
[76] U. Baul, D. Chakraborty, M. L. Mugnai, J. E. Straub, D. Thirumalai, *J. Phys. Chem. B* **2019**, *123*, 3462–3474.
[77] A. Pandey, M. Mann, *Nature* **2000**, *405*, 837–846.
[78] C. Bayard, F. Lottspeich, *J. Chromatogr. B* **2001**, *756*, 113–122.
[79] R. Kellner, *Fresenius J. Anal. Chem.* **2000**, *366*, 517–524.
[80] A. Görg, W. Weiss, M. J. Dunn, *Proteomics* **2004**, *4*, 3665–3685.
[81] K. Gevaert, J. Vandekerckhove, *Electrophoresis* **2000**, *21*, 1145–1154.
[82] S. Tamara, M. A. den Boer, A. J. R. Heck, *Chem. Rev.* **2022**, *122*, 7269–7326.
[83] J. Wen, T. Arakawa, J. S. Philo, *Anal. Biochem.* **1996**, *240*, 155–166.
[84] P. Rösch, *J. Chromatogr. B* **2001**, *756*, 165–177.
[85] M. S. Smyth, *Mol. Pathol.* **2000**, *53*, 8–14.
[86] Y. Jiang, C. G. Kalodimos, *J. Mol. Biol.* **2017**, *429*, 2667–2676.
[87] T. K. S. Kumar, C. Yu, *Acc. Chem. Res.* **2004**, *37*, 929–936.
[88] A. G. Kikhney, D. I. Svergun, *FEBS Lett.* **2015**, *589*, 2570–2577.
[89] S. Akiyama, S. Takahashi, T. Kimura, K. Ishimori, I. Morishima, Y. Nishikawa, T. Fujisawa, *Proc. Nat. Acad. Sci.* **2002**, *99*, 1329–1334.
[90] T. Mittag, J. D. Forman-Kay, *Curr. Opin. Struct. Biol.* **2007**, *17*, 3–14.
[91] R. Lazim, D. Suh, S. Choi, *Int. J. Mol. Sci.* **2020**, *21*, 6339.
[92] N. C. Nielsen, A. Malmendal, T. Vosegaard, *Mol. Membr. Biol.* **2004**, *21*, 129–141.
[93] R. De Zorzi, W. Mi, M. Liao, T. Walz, *Microscopy* **2016**, *65*, 81–96.
[94] B. A. Wallace, *Q. Rev. Biophys.* **2009**, *42*, 317–370.
[95] S. M. Kelly, T. J. Jess, N. C. Price, *Biochim. Biophys. Acta Proteins Proteomics* **2005**, *1751*, 119–139.
[96] S. Kelly, N. Price, *Curr. Protein Pept. Sci.* **2000**, *1*, 349–384.
[97] L. Konermann, J. Pan, Y.-H. Liu, *Chem. Soc. Rev.* **2011**, *40*, 1224–1234.
[98] G. H. Beaven, E. R. Holiday, in *Adv. Protein Chem.* (Eds.: M. L. Anson, K. Bailey, J. T. Edsall), Academic Press, **1952**, pp. 319–386.
[99] H. Chen, E. Rhoades, *Curr. Opin. Struct. Biol.* **2008**, *18*, 516–524.
[100] C. M. Johnson, *Arch. Biochem. Biophys.* **2013**, *531*, 100–109.
[101] B. N. G. Giepmans, *Histochem. Cell Biol.* **2008**, *130*, 211.

[102] B. J. G. E. Pieters, M. B. van Eldijk, R. J. M. Nolte, J. Mecinović, *Chem. Soc. Rev.* **2016**, *45*, 24–39.
[103] K. Henzler-Wildman, D. Kern, *Nature* **2007**, *450*, 964–972.
[104] P. Csermely, R. Palotai, R. Nussinov, *Trends Biochem. Sci.* **2010**, *35*, 539–546.
[105] H. H. Guo, J. Choe, L. A. Loeb, *Proc. Nat. Acad. Sci.* **2004**, *101*, 9205–9210.
[106] F. Nastri, D. D'Alonzo, L. Leone, G. Zambrano, V. Pavone, A. Lombardi, *Trends Biochem. Sci.* **2019**, *44*, 1022–1040.
[107] Q. Liu, G. Xun, Y. Feng, *Biotechnol. Adv.* **2019**, *37*, 530–537.
[108] L. F. Ribeiro, V. Amarelle, L. D. F. Alves, G. M. V. de Siqueira, G. L. Lovate, T. C. Borelli, M.-E. Guazzaroni, *Molecules* **2019**, *24*, 2879–2903.
[109] F. Rosati, G. Roelfes, *ChemCatChem* **2010**, *2*, 916–927.
[110] U. Markel, D. F. Sauer, J. Schiffels, J. Okuda, U. Schwaneberg, *Angew. Chem. Int. Ed.* **2019**, *58*, 4454–4464.
[111] A. Sharma, G. Gupta, T. Ahmad, S. Mansoor, B. Kaur, *Food Rev. Int.* **2021**, *37*, 121–154.
[112] E. Kuah, S. Toh, J. Yee, Q. Ma, Z. Gao, *Chem. A Eur. J.* **2016**, *22*, 8404–8430.
[113] J. McCafferty, A. D. Griffiths, G. Winter, D. J. Chiswell, *Nature* **1990**, *348*, 552.
[114] T. Heinisch, T. R. Ward, *Curr. Opin. Chem. Biol.* **2010**, *14*, 184–199.
[115] M. I. Sadowski, D. T. Jones, *Curr. Opin. Struct. Biol.* **2009**, *19*, 357–362.
[116] K. Chen, F. H. Arnold, *Nat. Catal.* **2020**, *3*, 203–213.
[117] F. H. Arnold, *Angew. Chem. Int. Ed.* **2019**, *58*, 14420–14426.
[118] The Royal Swedish Academy of Sciences, *Scientific Background on the Nobel Prize in Chemistry 2018 - Directed Evolution of Enzymes and Binding Proteins*, **2018**.
[119] M. Smith, *Biosci. Rep.* **1994**, *14*, 51–66.
[120] C. A. Hutchison, S. Phillips, M. H. Edgell, S. Gillam, P. Jahnke, M. Smith, *J. Biol. Chem.* **1978**, *253*, 6551–6560.
[121] U. T. Bornscheuer, B. Hauer, K. E. Jaeger, U. Schwaneberg, *Angew. Chem. Int. Ed.* **2019**, *58*, 36–40.
[122] D. L. Trudeau, D. S. Tawfik, *Curr. Opin. Biotechnol.* **2019**, *60*, 46–52.
[123] R. Frey, T. Hayashi, R. M. Buller, *Curr. Opin. Biotechnol.* **2019**, *60*, 29–38.
[124] U. T. Bornscheuer, *Philos. Trans. R. Soc. London* **2018**, *376*, 1–7.
[125] C. Zeymer, D. Hilvert, *Annu. Rev. Biochem.* **2018**, *87*, 131–157.
[126] M. Jeschek, R. Reuter, T. Heinisch, C. Trindler, J. Klehr, S. Panke, T. R. Ward, *Nature* **2016**, *537*, 661–665.
[127] Z. Xu, Y.-K. Cen, S.-P. Zou, Y.-P. Xue, Y.-G. Zheng, *Crit. Rev. Biotechnol.* **2020**, *40*, 83–98.
[128] C. Ren, X. Wen, J. Mencius, S. Quan, *Bioresour. Bioprocess.* **2019**, *6*, 53.
[129] G. Hattori, Y. Hirai, M. Sawamoto, T. Terashima, *Polym. Chem.* **2017**, *8*, 7248–7259.
[130] A. P. P. Kröger, M. I. Komil, N. M. Hamelmann, A. Juan, M. H. Stenzel, J. M. J. Paulusse, *ACS Macro Lett.* **2019**, *8*, 95–101.
[131] Z. Cui, H. Cao, Y. Ding, P. Gao, X. Lu, Y. Cai, *Polym. Chem.* **2017**, *8*, 3755–3763.
[132] H. Yamamoto, Y. Morishima, *Macromolecules* **1999**, *32*, 7469–7475.
[133] J. Chen, J. Wang, Y. Bai, K. Li, E. S. Garcia, A. L. Ferguson, S. C. Zimmerman, *J. Am. Chem. Soc.* **2018**, *140*, 13695–13702.
[134] H. K. Murnen, A. R. Khokhlov, P. G. Khalatur, R. A. Segalman, R. N. Zuckermann, *Macromolecules* **2012**, *45*, 5229–5236.
[135] H. S. Ashbaugh, *J. Phys. Chem. B* **2009**, *113*, 14043–14046.
[136] P. G. Khalatur, V. A. Ivanov, N. P. Shusharina, A. R. Khokhlov, *Russ. Chem. Bull.* **1998**, *47*, 855–860.
[137] Y. Chang, C. L. McCormick, *Macromolecules* **1993**, *26*, 6121–6126.
[138] H. Yamamoto, I. Tomatsu, A. Hashidzume, Y. Morishima, *Macromolecules* **2000**, *33*, 7852–7861.
[139] H. Yamamoto, M. Mizusaki, K. Yoda, Y. Morishima, *Macromolecules* **1998**, *31*, 3588–3594.
[140] S. L. Hilburg, Z. Ruan, T. Xu, A. Alexander-Katz, *Macromolecules* **2020**, *53*, 9187–9199.
[141] T. Terashima, T. Sugita, K. Fukae, M. Sawamoto, *Macromolecules* **2014**, *47*, 589–600.
[142] Y. Hirai, T. Terashima, M. Takenaka, M. Sawamoto, *Macromolecules* **2016**, *49*, 5084–5091.
[143] M. Mizusaki, Y. Morishima, F. M. Winnik, *Macromolecules* **1999**, *32*, 4317–4326.
[144] G. M. ter Huurne, L. N. J. de Windt, Y. Liu, E. W. Meijer, I. K. Voets, A. R. A. Palmans, *Macromolecules* **2017**, *50*, 8562–8569.
[145] Y. Abdouni, G. M. ter Huurne, G. Yilmaz, A. Monaco, C. Redondo-Gómez, E. Meijer, A. R. A. Palmans, C. R. Becer, *Biomacromolecules* **2021**, *22*, 661–670.
[146] Z. Li, M. Tang, S. Liang, M. Zhang, G. M. Biesold, Y. He, S.-M. Hao, W. Choi, Y. Liu, J. Peng, Z. Lin, *Prog. Polym. Sci.* **2021**, *116*, 101387.
[147] J. C. Foster, S. Varlas, B. Couturaud, Z. Coe, R. K. O'Reilly, *J. Am. Chem. Soc.* **2019**, *141*, 2742–2753.
[148] G. D. Rose, P. J. Fleming, J. R. Banavar, A. Maritan, *Proc. Nat. Acad. Sci.* **2006**, *103*, 16623–16633.
[149] B.-C. Lee, R. N. Zuckermann, K. A. Dill, *J. Am. Chem. Soc.* **2005**, *127*, 10999–11009.
[150] A. A. Fuller, C. J. Jimenez, E. K. Martinetto, J. L. Moreno, A. L. Calkins, K. M. Dowell, J. Huber, K. N. McComas, A. Ortega, *Front. Chem.* **2020**, *8*, 1–13.
[151] P. J. M. Stals, M. A. J. Gillissen, R. Nicolaÿ, A. R. A. Palmans, E. W. Meijer, *Polym. Chem.* **2013**, *4*, 2584–2597.
[152] R. C. W. Liu, A. Pallier, M. Brestaz, N. Pantoustier, C. Tribet, *Macromolecules* **2007**, *40*, 4276–4286.
[153] Y. Ogura, M. Artar, A. R. A. Palmans, M. Sawamoto, E. W. Meijer, T. Terashima, *Macromolecules* **2017**, *50*, 3215–3223.
[154] G. M. ter Huurne, M. A. J. Gillissen, A. R. A. Palmans, I. K. Voets, E. W. Meijer, *Macromolecules* **2015**, *48*, 3949–3956.
[155] N. Hosono, M. A. J. Gillissen, Y. Li, S. S. Sheiko, A. R. A. Palmans, E. W. Meijer, *J. Am. Chem. Soc.* **2013**, *135*, 501–510.
[156] A. M. Rosales, H. K. Murnen, S. R. Kline, R. N. Zuckermann, R. A. Segalman, *Soft Matter* **2012**, *8*, 3673.
[157] T. Terashima, T. Mes, T. F. A. de Greef, M. A. J. Gillissen, P. Besenius, A. R. A. Palmans, E. W. Meijer, *J. Am. Chem. Soc.* **2011**, *133*, 4742–4745.
[158] J. L. Warren, P. A. Dykeman-Bermingham, A. S. Knight, *J. Am. Chem. Soc.* **2021**, *143*, 13228–13234.
[159] H. Yamamoto, A. Hashidzume, Y. Morishima, *Polym. J.* **2000**, *32*, 745–752.
[160] K. Matsumoto, T. Terashima, T. Sugita, M. Takenaka, M. Sawamoto, *Macromolecules* **2016**, *49*, 7917–7927.
[161] O. Altintas, M. Artar, G. ter Huurne, I. K. Voets, A. R. A. Palmans, C. Barner-Kowollik, E. W. Meijer, *Macromolecules* **2015**, *48*, 8921–8932.
[162] E. A. Appel, J. Dyson, J. Delbarrio, Z. Walsh, O. A. Scherman, J. del Barrio, Z. Walsh, O. A. Scherman, *Angew. Chem. Int. Ed.* **2012**, *51*, 4185–4189.
[163] Z. Zhu, N. Xu, Q. Yu, L. Guo, H. Cao, X. Lu, Y. Cai, *Macromol. Rapid Commun.* **2015**, *36*, 1521–1527.
[164] F. Wang, H. Pu, M. Jin, D. Wan, *Macromol. Rapid Commun.* **2016**, *37*, 330–336.
[165] S. Mavila, O. Eivgi, I. Berkovich, N. G. Lemcoff, *Chem. Rev.* **2016**, *116*, 878–961.
[166] J. He, L. Tremblay, S. Lacelle, Y. Zhao, *Soft Matter* **2011**, *7*, 2380–2386.
[167] H. Zhang, L. Zhang, J. You, N. Zhang, L. Yu, H. Zhao, H.-J. Qian, Z.-Y. Lu, *CCS Chem.* **2020**, *3*, 2143–2154.
[168] C. Song, L. Li, L. Dai, S. Thayumanavan, *Polym. Chem.* **2015**, *6*, 4828–4834.
[169] D. E. Whitaker, C. S. Mahon, D. A. Fulton, *Angew. Chem. Int. Ed.* **2013**, *52*, 956–959.
[170] N. Ormategui, I. García, D. Padro, G. Cabañero, H. J. Grande, I. Loinaz, *Soft Matter* **2012**, *8*, 734–740.
[171] Y. Bai, H. Xing, G. A. Vincil, J. Lee, E. J. Henderson, Y. Lu, N. G. Lemcoff, S. C. Zimmerman, *Chem. Sci.* **2014**, *5*, 2862–2868.
[172] E. H. H. Wong, S. J. Lam, E. Nam, G. G. Qiao, *ACS Macro Lett.* **2014**, *3*, 524–528.
[173] H. Chang, M. Shi, Y. Sun, J. Jiang, *Chin. J. Polym. Sci.* **2015**, *33*, 1086–1095.
[174] M. Matsumoto, T. Terashima, K. Matsumoto, M. Takenaka, M. Sawamoto, *J. Am. Chem. Soc.* **2017**, *139*, 7164–7167.
[175] S. Wijker, L. Deng, F. Eisenreich, I. K. Voets, A. R. A. Palmans, *Macromolecules* **2022**, *55*, 6220–6230.
[176] T.-C. Chang, K. Tanaka, *Bioorg. Med. Chem.* **2021**, *46*, 116353.
[177] A. P. P. Kröger, J. M. J. Paulusse, *J. Controlled Release* **2018**, *286*, 326–347.
[178] C.-C. Cheng, F.-C. Chang, H.-C. Yen, D.-J. Lee, C.-W. Chiu, Z. Xin, *ACS Macro Lett.* **2015**, *4*, 1184–1188.
[179] L. Deng, L. Albertazzi, A. R. A. Palmans, *Biomacromolecules* **2022**, *23*, 326–338.
[180] S. Wijker, R. Monnink, L. Rijnders, L. Deng, A. R. A. Palmans, *Chem. Commun.* **2023**, *59*, 5407–5410.
[181] P. Theato, *J. Polym. Sci. Part A* **2008**, *46*, 6677–6687.
[182] Y. Liu, T. Pauloehrl, S. I. Presolski, L. Albertazzi, A. R. A. Palmans, E. W. Meijer, *J. Am. Chem. Soc.* **2015**, *137*, 13096–13105.
[183] R. Upadhya, N. S. Murthy, C. L. Hoop, S. Kosuri, V. Nanda, J. Kohn, J. Baum, A. J. Gormley, *Macromolecules* **2019**, *52*, 8295–8304.

[184] J. Engelke, J. Brandt, C. Barner-Kowollik, A. Lederer, *Polym. Chem.* **2019**, *10*, 3410–3425.
[185] P. Groves, *Polym. Chem.* **2017**, *8*, 6700–6708.
[186] T. S. Fischer, D. Schulze-Sünninghausen, B. Luy, O. Altintas, C. Barner-Kowollik, *Angew. Chem. Int. Ed.* **2016**, *55*, 11276–11280.
[187] K. Kirshenbaum, A. E. Barron, R. A. Goldsmith, P. Armand, E. K. Bradley, K. T. V. Truong, K. A. Dill, F. E. Cohen, R. N. Zuckermann, *Proc. Nat. Acad. Sci.* **1998**, *95*, 4303–4308.
[188] M. Nagao, Y. Miura, *ACS Macro Lett.* **2023**, *12*, 733–737.
[189] Y. Morishima, K. Saegusa, M. Kamachi, *Macromolecules* **1995**, *28*, 1203–1207.
[190] M. C. A. Stuart, J. C. Van De Pas, J. B. F. N. Engberts, *J. Phys. Org. Chem.* **2005**, *18*, 929–934.
[191] P. J. M. Stals, C.-Y. Cheng, L. Van Beek, A. C. Wauters, A. R. A. Palmans, S. Han, E. W. Meijer, *Chem. Sci.* **2016**, *7*, 2011–2015.
[192] J. F. Thümmler, A. H. Roos, J. Krüger, D. Hinderberger, F. Schmitt, G. Tang, F. G. Golmohamadi, J. Laufer, W. H. Binder, *Macromol. Rapid Commun.* **2023**, *44*, 2200618.
[193] J. F. Hoffmann, A. H. Roos, F. Schmitt, D. Hinderberger, W. H. Binder, *Angew. Chem. Int. Ed.* **2021**, *60*, 7820–7827.
[194] A. H. Roos, J. F. Hoffmann, W. H. Binder, D. Hinderberger, *Soft Matter* **2021**, *17*, 7032–7037.
[195] E. Archontakis, L. Deng, P. Zijlstra, A. R. A. Palmans, L. Albertazzi, *J. Am. Chem. Soc.* **2022**, *144*, 23698–23707.
[196] A. Latorre-Sánchez, J. A. Pomposo, *Polym. Int.* **2016**, *65*, 855–860.
[197] M. T. De Martino, L. K. E. A. Abdelmohsen, F. P. J. T. Rutjes, J. C. M. van Hest, *Beilstein J. Org. Chem.* **2018**, *14*, 716–733.
[198] T. Terashima, M. Ouchi, T. Ando, M. Kamigaito, M. Sawamoto, *Macromolecules* **2007**, *40*, 3581–3588.
[199] T. Terashima, M. Ouchi, T. Ando, M. Sawamoto, *J. Polym. Sci. Part A* **2010**, *48*, 373–379.
[200] J. Rubio-Cervilla, E. González, J. Pomposo, *Nanomaterials* **2017**, *7*, 341.
[201] F. Eisenreich, A. R. A. Palmans, in *Supramol. Catal.* (Eds.: P. W. N. M. van Leeuwen, M. Raynal), Wiley, **2022**, pp. 489–506.
[202] A. Sathyan, L. Deng, T. Loman, A. R. A. Palmans, *Catal. Today* **2023**, *418*, 114116.
[203] E. Huerta, P. J. M. Stals, E. W. Meijer, A. R. A. Palmans, *Angew. Chem.* **2013**, *125*, 2978–2982.
[204] Y. Liu, S. Pujals, P. J. M. Stals, T. Paulöhrl, S. I. Presolski, E. W. Meijer, L. Albertazzi, A. R. A. Palmans, *J. Am. Chem. Soc.* **2018**, *140*, 3423–3433.
[205] A. Sathyan, S. Croke, A. M. Pérez-López, B. F. M. de Waal, A. Unciti-Broceta, A. R. A. Palmans, *Mol. Syst. Des. Eng.* **2022**, *7*, 1736–1748.
[206] E. S. Garcia, T. M. Xiong, A. Lifschitz, S. C. Zimmerman, *Polym. Chem.* **2021**, *12*, 6755–6760.
[207] J. Chen, K. Li, S. E. Bonson, S. C. Zimmerman, *J. Am. Chem. Soc.* **2020**, *142*, 13966–13973.
[208] J. Chen, K. Li, J. S. Shon, S. C. Zimmerman, *J. Am. Chem. Soc.* **2020**, *142*, 4565–4569.
[209] R. Huang, C.-H. Li, R. Cao-Milán, L. D. He, J. M. Makabenta, X. Zhang, E. Yu, V. M. Rotello, *J. Am. Chem. Soc.* **2020**, *142*, 10723–10729.
[210] I. Perez-Baena, I. Loinaz, D. Padro, I. García, H. J. Grande, I. Odriozola, *J. Mater. Chem.* **2010**, *20*, 6916–6922.
[211] A. P. P. Kröger, N. M. Hamelmann, A. Juan, S. Lindhoud, J. M. J. Paulusse, *ACS Appl. Mater. Interfaces* **2018**, *10*, 30946–30951.
[212] N. M. Hamelmann, J.-W. D. Paats, Y. Avalos-Padilla, E. Lantero, L. Spanos, I. Siden-Kiamos, X. Fernàndez-Busquets, J. M. J. Paulusse, *ACS Infect. Dis.* **2023**, *9*, 56–64.
[213] A. B. Benito, M. K. Aiertza, M. Marradi, L. Gil-Iceta, T. Shekhter Zahavi, B. Szczupak, M. Jiménez-González, T. Reese, E. Scanziani, L. Passoni, M. Matteoli, M. De Maglie, A. Orenstein, M. Oron-Herman, G. Kostenich, L. Buzhansky, E. Gazit, H.-J. J. Grande, V. Gómez-Vallejo, J. Llop, I. Loinaz, *Biomacromolecules* **2016**, *17*, 3213–3221.
[214] B. Panganiban, B. Qiao, T. Jiang, C. DelRe, M. M. Obadia, T. D. Nguyen, A. A. A. Smith, A. Hall, I. Sit, M. G. Crosby, P. B. Dennis, E. Drockenmuller, M. Olvera de la Cruz, T. Xu, *Science* **2018**, *359*, 1239–1243.
[215] T. Jiang, A. Hall, M. Eres, Z. Hemmatian, B. Qiao, Y. Zhou, Z. Ruan, A. D. Couse, W. T. Heller, H. Huang, M. O. de la Cruz, M. Rolandi, T. Xu, *Nature* **2020**, *577*, 216–220.
[216] S. Funtan, Z. Evgrafova, J. Adler, D. Huster, W. Binder, *Polymer* **2016**, *8*, 178.
[217] Z. Evgrafova, B. Voigt, A. H. Roos, G. Hause, D. Hinderberger, J. Balbach, W. H. Binder, *Phys. Chem. Chem. Phys.* **2019**, *21*, 20999–21006.
[218] Z. Evgrafova, B. Voigt, M. Baumann, M. Stephani, W. H. Binder, J. Balbach, *ChemPhysChem* **2019**, *20*, 236–240.
[219] Z. Evgrafova, S. Rothemund, B. Voigt, G. Hause, J. Balbach, W. H. Binder, *Macromol. Rapid Commun.* **2020**, *41*, 1900378.
[220] N. Sen, G. Hause, W. H. Binder, *Macromol. Rapid Commun.* **2021**, *42*, 2100120.
[221] E. Verde-Sesto, A. Arbe, A. J. Moreno, D. Cangialosi, A. Alegría, J. Colmenero, J. A. Pomposo, *Mater. Horiz.* **2020**, *7*, 2292–2313.

Manuscript received: May 31, 2023
Revised manuscript received: July 6, 2023
Accepted manuscript online: July 7, 2023
Version of record online: ■■, ■■